Experimental evaluation of Kalman filter based MPPT in grid-connected PV system

Majd Chellal

Supervised by

Prof. Vicente Leite

Dr. Hafidha Sebbagh

Bragança

2020-2021

Experimental evaluation of Kalman filter based MPPT in grid-connected PV system

Master in Renewable Energy and Energy Efficiency

School of Technology and Management of the Polytechnic Institute of Bragança

Majd Chellal

2020-2021

I declare that the work described in this report is of my own authorship and it is my wish that it be submitted for evaluation.

Majd Chellal

Dedication

With the expression of my gratitude, I dedicate this modest work to whom, whatever the terms embraced, I never manage to express my sincere love to them.

To the man, my precious offer of the god, who owes my life, my success and all my respect: my lovely father.

To the woman who has suffered without letting me suffer, who has spared no effort to make me happy: my lovely mother.

To my dear and adorable brothers and sisters.
As a symbol of my fraternal affection, my deep tenderness and gratitude, I wish you a life full of happiness and success and may God, the Almighty, protect and guard you.

Acknowledgment

I thank ALLAH the merciful for giving us, always the patience and the faith to reach our goals.

I would like to acknowledge my supervisor, Prof. Américo Vicente Leite for the motivation, criticism and honesty, which have been of immense help for the evolution as a person and as a student who wants to achieve his goals. I would also like to thank my mentor co-supervisor from Algeria Dr. Hafidha Sebbagh for the support, advice and guidance throughout this thesis.

I would also like to express my sincere appreciation to all my master professors either at the Polytechnic Institute of Bragança and at the Superior School of Applied Sciences of Tlemcen, especially Dr. Boukli Fouad for their contribution to achieve this goal and for the preparation processes related to coming to Portugal.

I am grateful to all my friends, especially Yacoub Sallam, Abdessalam Garmat and Arezki Abderrahim Chellal. Also, my thanks to my colleague Thiago Fialho Guimarães with whom I shared the IPB research laboratory.

Finally, I would also like to thank all those who contributed directly or indirectly to the development of this document.

Abstract

Photovoltaic (PV) energy is becoming an important alternative energy source, since it is abundant in nature, non-polluting and requires low maintenance. However, it suffers from low energy conversion efficiency, which can be even lower if the photovoltaic generator does not operate around a so-called Maximum Power Point (MPP). Tracking this point, which changes its location depending on weather conditions, is a very important step in the design of a photovoltaic system. Several techniques have been investigated in the literature in the MPP context. However, some techniques such as the Kalman filter are steel unknown with a lack of information in real test conditions, since their evaluation is limited only in simulation and literature review. This work presents an experimental evaluation of the Kalman filter based on a comparison with two well-known maximum power point tracking (MPPT) algorithms, which are the Perturbation and observation (among the simplest techniques) and the Particle Swarm Optimization (among the most complex techniques). The experimental tests were carried out under real atmospheric conditions, using Matlab/Simulink and the 1103 dSPACE real-time controller board. The results show that the Kalman filter has a higher aptitude to operate closer to the MPP, with a low oscillation in steady-state compared to the other MPPT evaluated in this work. However, the technique's flaw lies in the shadow situation where it can not differentiate between the local and global optimums, unlike the particle swarm optimization.

Keywords: Photovoltaic (PV), Maximum Power Point Tracking (MPPT), Perturbation and Observation (PO), Particle swarm optimization (PSO), Kalman Filter (KF), Grid connected PV system, dSPACE 1103.

Resumo

A energia fotovoltaica (PV) está a tornar-se uma importante fonte de energia alternativa, uma vez que é abundante na natureza, não poluente, e requer pouca manutenção. No entanto, sofre de uma baixa eficiência de conversão energética, que pode ser ainda mais baixa se o gerador PV não operar em torno do chamado Ponto de Potência Máxima (MPP). O rastreio deste ponto, que muda a sua localização dependendo das condições meteorológicas, é um passo muito importante na concepção de um sistema PV. Várias técnicas têm sido investigadas na literatura no contexto do MPP. No entanto, o desempenho de algumas técnicas, como o filtro Kalman, em condições reais de teste, ainda desconhecido, ou existe pouca informação, uma vez que a sua avaliação é limitada apenas na simulação e revisão da literatura. Este trabalho apresenta uma avaliação experimental do filtro de Kalman com base numa comparação com dois seguidores de ponto de potência máxima (MPPT) bem conhecidos, que são a Perturbação e observação e a Optimização do Enxame de Partículas. Os testes experimentais foram realizados em condições atmosféricas reais, utilizando o Matlab/Simulink e a carta de controlo em tempo real dSPACE. Os resultados mostram que o filtro de Kalman tem uma maior aptidão para operar mais perto do MPP, com uma baixa oscilação em regime permenente, comparativemente com os outros algoritmos MPPT avaliados neste trabalho. No entanto, a desvantagem ocorre aquando da ocorância de sombra, onde a técnica não consegue diferenciar entre os óptimos locais e global, ao contrário da optimização do enxame de partículas.

Palavras-chave: Fotovoltaico (PV), Seguimento do Ponto de Potência Máxima (MPPT), Perturbação e Observação (PO), Optimização de enxame de partículas (PSO), Filtro de Kalman (KF), Sistema PV ligado à Rede, dSPACE 1103.

الملخص

أصبحت الطاقة الكهروضوئية (PV) مصدرًا مهمًا للطاقة البديلة ، لأنها وفيرة في الطبيعة وغير ملوثة وتتطلب صيانة منخفضة. ومع ذلك ، فإنها تعاني من كفاءة تحويل منخفضة للطاقة ، والتي يمكن أن تكون أقل إذا كان المولد الكهروضوئي لا يعمل حول ما يسمى نقطة الطاقة القصوى . يعد تتبع هذه النقطة ، التي تغير موقعها اعتمادًا على الظروف الجوية ، خطوة مهمة جدًا في تصميم النظام الكهروضوئي. تم التحقيق في العديد من التقنيات في المنشورات الموجودة سابقا في سياق تتبع نقطة الطاقة القصوى . ومع ذلك ، فإن بعض التقنيات مثل مرشح كالمان تظل غير معروفة مع نقص المعلومات في ظروف الاختبار الحقيقية ، نظرًا لأن تقييمها السابق محدود فقط في المحاكاة ومراجعة الأدبيات. يقدم هذا العمل تقييمًا تجريبيًا لمرشح كالمان استنادًا إلى مقارنة مع تقنيتين معروفتين لتتبع نقطة الطاقة القصوى ، وهما الاضطراب والمراقبة (أحد أبسط التقنيات) وتحسين سرب الجسيمات (أحد أكثر التقنيات تعقدا). تم إجراء الاختبارات التجريبية في ظل ظروف جوية حقيقية ، باستخدام Matlab / Simulink ولوحة التحكم في الوقت الحقيقي dSPACE 1103. أظهرت النتائج أن مرشح كالمان يتمتع بقدرة أعلى على العمل بالقرب من الطاقة القصوى ، مع تذبذب منخفض في حالة الاستقرار مقارنةً بالتقنيات الأخرى التي تم تقييمها في هذا العمل. ومع ذلك ، فإن عيب التقنية موجود في حالة الظل حيث لا يمكن للتقنية التمييز بين القيم المثلى المحلية والكلية ، على عكس تقنية تحسين سرب الجسيمات.

كلمات مفتاحية : الانظمة الكهروضوئية (PV) ، تتبع نقطة الطاقة القصوى (MPPT) ، الاضطراب والملاحظة (P&O) ، تحسين سرب الجسيمات (PSO) ، مرشح كالمان (KF) ، النظام الكهروضوئي المتصل بالشبكة ، dSPACE 1103.

Contents

List of Tables

List of Figures

Acronyms

AC	Alternative Current
DC	Direct Current
$ESTiG$	Escola Superior de Tecnologia e Gestão
IPB	Instituto Politécnico de Bragança
$IGBT$	Insulated Gate Bipolar Transistor
$GMPP$	Global Maximum Power Point
KF	Kalman Filter
$LMPP$	Local Maximum Power Point
MPP	Maximum Power Point
$MPPT$	Maximum Power Point Tracking
$MLPEs$	Module Level Power Electronics
$NOCT$	Normal Operating Cell Temperature
PSO	Particle Swarm Optimisation
PO	Pertubation and Observation
PV	Photovoltaic
PLL	Phase Locked Loop
PID	Proportional-Integral-Derivative controller
STC	Standard Test Condition
VOC	Voltage Oriented Control
VSI	Voltage Source Inverter

Symbols

I_{cc}	Short-circuited current
V_{oc}	Open circuit voltage
V_{pv}	The PV output voltage
I_{pv}	The PV output current
P_{pv}	The PV output power
I_{MPP}	Current at maximum power point
V_{MPP}	Voltage at maximum power point
V_{ref}	Reference voltage
I_{ref}	Reference current
V_d	Voltage direct component
V_q	Voltage quadrature component
I_d	Current direct component
I_q	Current quadrature component
V_α	Voltage alpha component
V_β	Voltage beta component
I_α	Current alpha component
I_β	Current beta component
k_p	Proportional gain
k_i	Integration gain
I_L	The light generated current
I_D	The current lost due to recombination
I_{sh}	The current lost due to shunt resistance
I_0	The reverse saturation current
V_T	The thermal voltage

Chapter 1

Introduction

This chapter introduces the background and motivation established in this work, including a brief overview of the current standing of Maximum Power point (MPPT) techniques. This is followed by project's objectives attached with the main contribution of this work. At the end of this chapter, an outline of this master thesis is provided.

1.1 Background of study

The climatic and geographical conditions have a great influence on the validity and efficiency of all types of renewable resources based on various aspects according to each resource [1]. However, photovoltaic (PV) solar energy is the least influenced since the source is generously distributed on our planet. Additionally, PV systems offer standard concepts in the implementation phase [2], in order to produce electricity through solar energy easily, and without causing major environmental risks [3]. For these reasons, PV systems have taken an essential market in the field of energy production worldwide. Figure 1.1 shows the average annual growth rates of several renewable energies, where the solar PV have the higher growth rate compared to other renewable resources, achieving 120 GW in the end of 2019. In which it accounted for approximately 59% of the total renewable energy production from new generation assets [4].

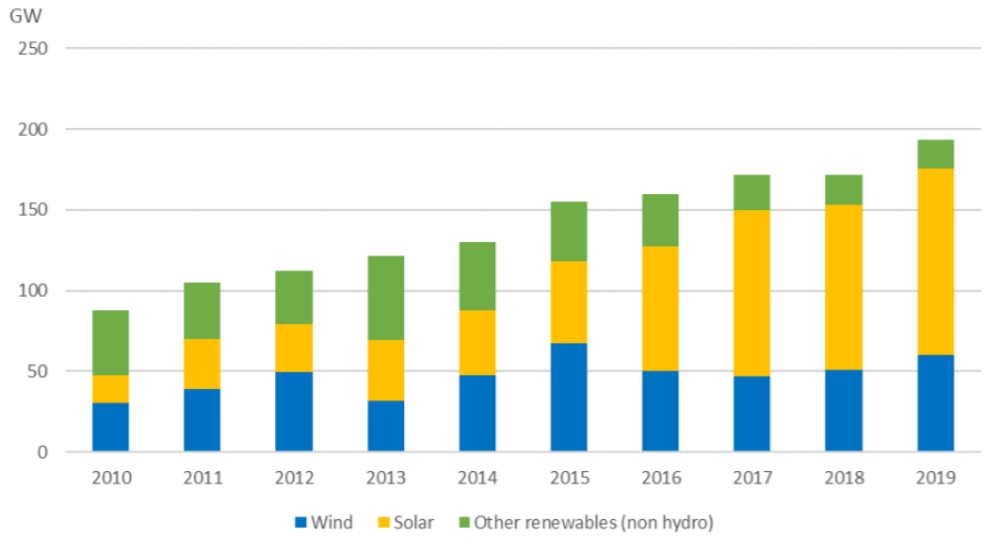

Figure 1.1: Average annual growth rates of renewable energy [4].

Additionally, according to the power density graph presented in Fig. 1.2, a PV efficiency close to 20% would translate to electricity generation rates between 20 and 40 W/m^2, i.e. one order of magnitude higher than the majority of wind and hydro projects, and two orders higher than biomass conversion [5].

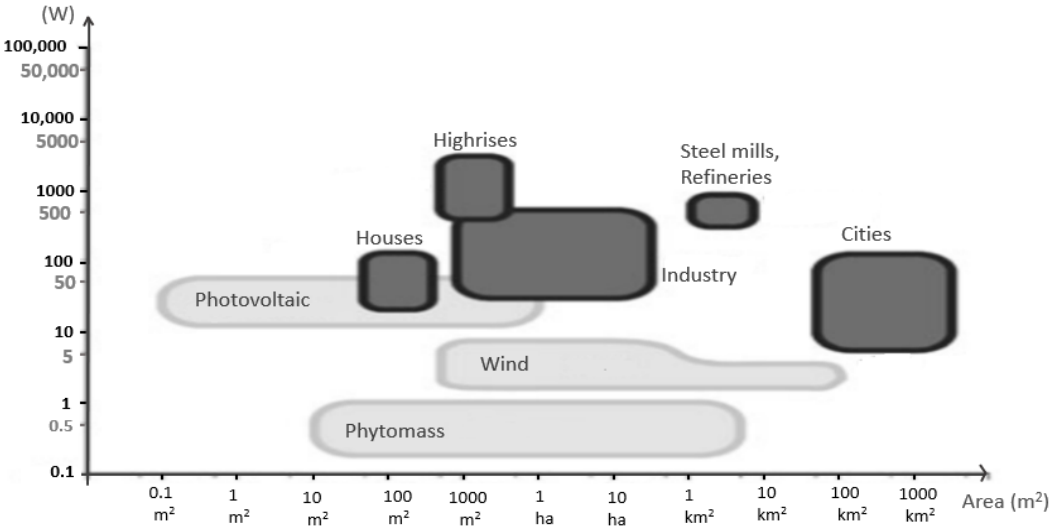

Figure 1.2: Power densities of energy consumption and renewable energy production [5].

From an economic point of view, the cost of energy generated by using PV systems is relatively high and cannot be competitive yet compared with traditional wholesale electricity prices, even thought the system efficiency remains low. However, the PV plant efficiency is greatly affected due to three factors:

- The efficiency of the inverter;
- The efficiency of the PV modules;
- The efficiency of the maximum power point tracking (MPPT) algorithms.

PV inverters available on the market based on silicon carbide (SiC) technology have improved efficiency around 98% [6], while improving the efficiency of the PV modules is hard because it may depend on the technology available which leads to a radical change in cost [7]. Instead, improving the efficiency of tracking the MPPT with several control techniques is easier. This motivates the research for evaluating some techniques in order to extract the maximum energy possible from a PV system.

1.2 Current standing of the maximum power point tracking

Since the 3^{th} century B.C. humanity has used solar power, primarily the Greeks bounced sunlight off of "burning mirrors" to light sacrosanct torches for their religious ceremonies. Despite this, the PV effect was uncovered very early in 1839 by the French scientist Edmond Becquerel. The first silicon PV cell has been developed at Bell Labs (America) in 1954 [8].

From 1954 to 2020, the maximum power point tracking (MPPT) is the aim of researchers to improve efficiency and enhance the yield of the PV systems, in which the control is based on electronic systems that varies the operating point of the PV module [9]. Nowadays, electrical MPPT techniques are employed in the majority of modern PV inverters. Their main function is to extract the maximum amount of energy available from the PV systems

during their period of functioning [10].

In other specific PV systems such as concentrator PV technology, mechanical sun-tracking system is required since this technology is mainly based on the direct solar radiation, through the use of high-efficiency cells and inexpensive polymer-lenses to concentrate the light on the cells. However, this category is complex and costly in implementation since it requires hydraulic cylinders and motors [9][11] .

1.3 Project motivation and objectives

The output power of PV systems is greatly affected by the external influences such as solar irradiation, temperature, shading effect, etc.... From this point, around 10 main MPPT techniques in literature have been evaluated in order to maintain the maximum efficiency of the PV systems [10]. However, some techniques such as the Kalman filter (KF) is still ambiguous since its evaluation is limited on simulations [12][13][14], which leads to a lack of credible information about its performance on tracking the maximum power in real conditions. Additionally, the initial parameterization presents the harsh task of the implementation, since a wrong initialization may diverge the tracking process away [15]. This creates a new challenge to evaluate the performance of the KF technique as well as the exploration of its advantages and disadvantages in real experimental tests. At this stage, this work aims to perform the operating principle of the KF and analyse its performances by comparing the concerned MPPT with two other well-known MPPTs, which are the perturbation and observation (one of the most simple techniques) and the particle swarm optimization (one of the most complex technique). The experimental results are performed in grid connected PV system, which consists of a PV array connected to the utility grid through a power conditioning block as shown in the block diagram of Fig. 1.3. The power conditioning topology includes a boost converter, MPPT block control, inverter, grid interface as well as the necessary control system for efficient system performance [16].

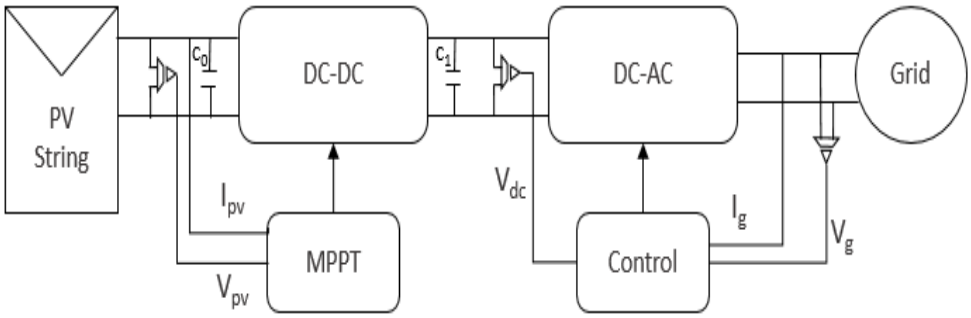

Figure 1.3: Block diagram of the PV system connected to the grid.

1.4 Main contribution

This work contributes to the validation of the Kalman filter-based MPPT in a grid-connected PV systems, by comparing this technique with two other algorithms of high utilization. An extension of this work was published in the International Journal of renewable Energy and Research (IJRER) [17]. The main contributions of this work can be summarized in the following items:

- **An understandable detail** covering the Kalman filter (KF), Perturbation and Observation (P&O) and the Particle Swarm optimization (PSO), which helps to differentiate between the operating principle of each MPPT algorithm, and identify the complexity of implementation, effectiveness, parameterization and sensors required.

- **Feasibility decision** based on two sets of experimental tests regarding the KF technique in the MPPT process. First, tests under normal operating conditions, where it is relevant to evaluate the accuracy in achieving the maximum power point (MPP), the oscillation around the MPP and the speed convergence. The second set of tests focuses on the ability to operate on the global MPP under partial shadow conditions.

1.5 Thesis organization

The thesis is divided into six chapters, which are briefly summarized in the following.

Chapter 2 presents the operating principle of PV cells and their main different types of crystalline silicon available in the market. Afterward, the mathematical model of the PV cell is presented, followed by the behavior of the PV modules imposed by the change of atmospheric conditions (temperature, radiance and even in partial shading). Finally, a brief description is provided about stand-alone and grid-connected PV systems in the MPPT context.

Chapter 3: starts with a literature review on the MPPT techniques, followed by a detailed explanation of the three MPPT experimented within this work, which are the Perturbation and observation (P&O), particle swarm optimization (PSO) and Kalman filter (KF).

Chapter 4: describes the power topology used for the experimental tests, including its relevant components. This chapter provides also the Simulink control blocks for the techniques evaluated in this work, attached with their required parametrization.

Chapter 5: presents the results obtained from the implementation of MPPT techniques, followed by performance analysis of their results.

Chapter 6: summarizes the work that has been achieved throughout this master thesis. The chapter ends with a perspective on the complementary research that can be carried out following the work presented in this project.

Chapter 2

Photovoltaic fundamentals

This chapter introduces the operating principle of photovoltaic (PV) cells, followed by their basic types. It provides also the mathematical model of the PV cells and the extent to which it is affected by external factors such as solar irradiance, temperature and shading. At the end, the profitability of the tracking of the maximum power point is provided for different types of PV installations.

2.1 Operating principle of a photovoltaic cell

The photovoltaic cell is a means of transforming light into electrical energy by using the photovoltaic effect process. The PV cell is made of two silicon layers, one P-doped (boron-doped) and the other layer N-doped (phosphorus-doped) providing a P-N junction with a potential barrier, as it is described in Fig. 2.1. When photons are absorbed by the semiconductor, they transmit their energy to the atoms of the P-N junction in such a way that electrons from these atoms are liberated and create electrons (negatively charged) and holes (positively charged), which creates a potential difference between the two layers. It is measured between the terminals of the positive and negative connections of the cell. The maximum voltage of the cell is about $0.45 - 0.58\ V$ at zero current [18], it is called the open circuit voltage V_{oc}. Whereas, the maximum current produced is the short-circuit current I_{cc} attained when the terminals of the cell are short-circuited.

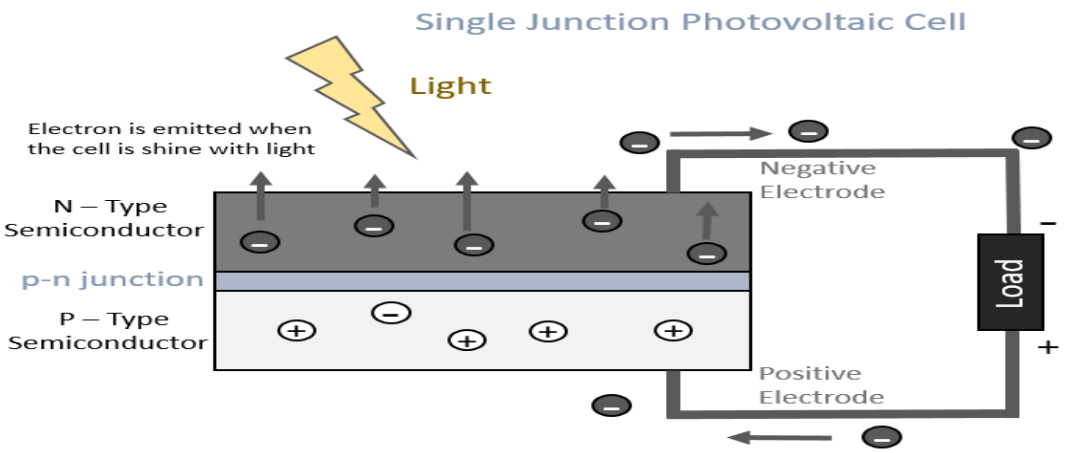

Figure 2.1: Schematic representation of a solar cell [18].

2.2 Basic Types of PV cells

Reference [19] presents a wide range of materials used for PV applications, such as the Cadmium telluride, Copper indium gallium selenide, Organic and polymer materials. However, crystalline silicon photovoltaic cells dominates the PV markets, since they are manufactured with different performances and forms, each model has its benefits compared to other models. The most commonly used types of crystalline silicon PV cells are shown in Fig. 2.2 [20], which are:

1. Mono-crystalline (single crystalline) cells:

   Mono-crystalline solar panels are generally considered as a premium product thanks to its high efficiency ($18-19\%$) and aesthetic performance. It is considered as the expensive crystalline silicon (0.83€ to 1.25€ per watt) [21][22].

2. Poly-crystalline (multi-crystalline) cells:

   It is made from the wafer cut of recrystallised silicon and as its name indicates, it is made up of a large number of crystals in a disordered manner. Poly-crystalline cells have a low efficiency (around $16-17\%$) compared to mono-crystalline cells, at a cost around 0.75€ to 0.83€ per watt [21][22].

3. Amorphous cells (Thin-film):

   It is formed by depositing a silicon film on a glass substrate. In this technology, less silicon is used in the production process compared to mono- or poly-crystalline cells, but this saving is at the detriment of the conversion efficiency (around 9%), which reflects its cost at 0.58€ to 0.83€ per watt [21][22].

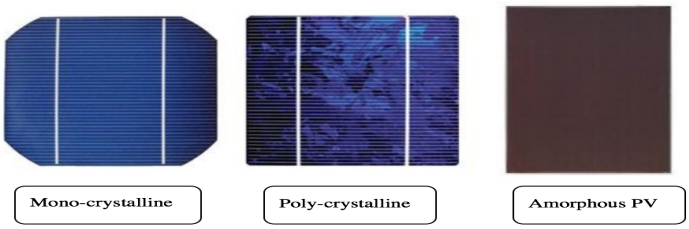

Figure 2.2: Different types of PV modules.

2.3 Equivalent circuit and mathematical model

The solar cells are represented based on diode models; single diode model [23][24], two diode model [25], and three diode model [26]. Generally, the single-diode model is the most widely used since it offers a good trade-off between simplicity and precision over other models. In the two-diode model, an additional diode is used to reflect the effect of carrier recombination. A three-diode model is applied to take into consideration the influence of grain boundaries and large leakage currents across the peripheries. The equivalent single diode circuit of the PV cell is represented in Fig. 2.3 [27] .

Using Kirchhoff's current law for current:

$$I = I_L - I_D - I_{sh}$$

Where I_L represents the light generated current in the cell (photocurrent), I_{sh} represents the current lost due to shunt resistances. In this circuit model, I_D represents the voltage-dependent current lost to recombination, it is formed using the Shockley model for an

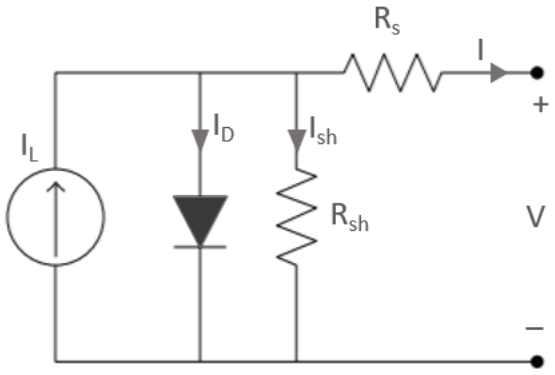

Figure 2.3: Single diode equivalent circuit models.

ideal unique diode by the following equation:

$$I_D = I_0 \left[exp\left(\frac{V + IR_s}{n * V_T} \right) - 1 \right] \tag{2.1}$$

Where n is the ideality factor of the diode, (the factor ideality is between 1 and 2 for a single junction cell), I_0 represents the reverse saturation current and V_T represents the thermal voltage as:

$$V_T = \frac{N_s K T_c}{q}$$

Where N_s is the number of cells in series, K is the Boltzmann's constant ($1.381 * 10^{-23} J/K$), q is the elementary charge ($1.602 * 10^{-19} C$) and T_c refers to the junction temperature of the module in Kelvin.

The shunt current can be written as:

$$I_{sh} = (V + (I * R_s))/R_{sh} \tag{2.2}$$

The parasitic parameters R_s and R_{sh} represent the series resistance and the shunt resistance, respectively. They affect the illuminated current–voltage (I-V) characteristics and efficiency of cells [28]. Therefore, using Eq. (2.1) and Eq. (2.2), the single diode circuit can be performed following Eq. (2.3).

$$I = I_L - I_0 \left[exp\left(\frac{V + IR_s}{n * V_T}\right) - 1 \right] - \frac{V + IR_s}{R_{sh}} \tag{2.3}$$

The output of the current source is instantly proportional to the light incident on the cell (photocurrent I_L) following Eq. (2.4). During darkness, the solar cells are not an active device, where it operates as a diode [29].

$$I_L = \frac{G}{G_{stc}} \times I_{sc} = \frac{G}{G_{stc}} \left(I_{sc,stc} + K_I \left(T - T_{stc}\right)\right) \tag{2.4}$$

In standard test condition (STC), the temperature T_{stc} and solar irradiance G_{stc} are respectively set at $298.15°K$ and $1000\, W/m^2$. Also, $I_{sc,stc}$ presents the short circuit current at standard test condition, and K_I is the short circuit temperature coefficient. The PV module temperature interferes with the solar irradiance (G) following Eq. (2.5).

$$T = T_{stc} + \frac{G}{G_{stc}} \times \left(\frac{NOCT - 20}{G_{0.8}}\right) = T_{stc} + G\left(\frac{NOCT - 20}{800}\right) \tag{2.5}$$

Where $NOCT$ refers to the normal operating temperature of the PV cell provided by the manufacturer in °C, it is defined as the temperature reached by open circuited cells in a module under the conditions listed below:

- Solar irradiance on cell surface = 800 W/m2;
- Air Temperature = 20C
- Wind Velocity = 1 m/s

The reverse saturation current of the diode, at the reference temperature, T_{stc}, is due to the diffusive flow of minority electrons from the p-side to the n-side and the minority holes from the n-side to the p-side, which can be expressed in Eq. (2.6).

$$I_{0,stc} = \frac{I_{sc,stc} - \frac{V_{oc}}{R_{sh}}}{exp\left(\frac{qV_{oc}}{nN_sKT_{stc}}\right) - 1} = \frac{I_{sc,stc} - \frac{V_{oc}}{R_{sh}}}{exp\left(\frac{V_{oc}}{nV_t}\right) - 1} \tag{2.6}$$

Hence, the reverse saturation current varies according to the diffusion coefficient of electrons and holes. As the minority carriers are thermally generated, the reverse saturation current is practically unaffected by the reverse bias but is strongly sensitive to temperature changes.

2.4 Non Linear characteristics of PV system

In Photovoltaic system, the output characteristics are largely dependent on the level of the irradiance and temperature. Based on Fig. 2.4.a, increasing the level of solar irradiance leads to increase the PV output current joined with a slight increase in the PV output voltage. While in Fig. 2.4.b, increasing the cell temperature leads to reduce the PV output voltage. It can be deduced that a photovoltaic cell generates a higher amount of output in the coldest place with a highest level of solar irradiation [30].

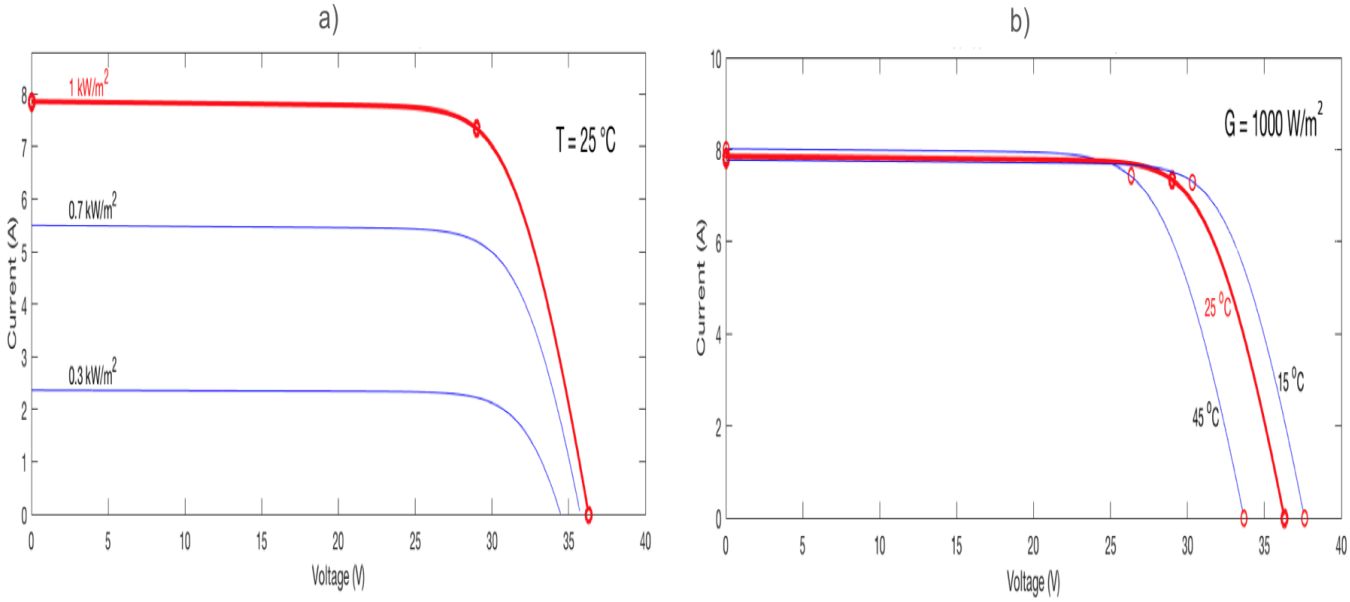

Figure 2.4: a) I-V curves of a PV module traced at different solar irradiance levels and 25°C; b) I-V curves of a PV module traced at different temperature levels and 1000 W/m^2.

Based on Fig. 2.5, the PV output power is directly proportional to the amount of solar irradiance falling on, and inversely proportional to the temperature. In addition, it

is clear that the change in atmospheric conditions implies a change in the position of the Maximum Power Point (MPP), which leads to affect the system efficiency.

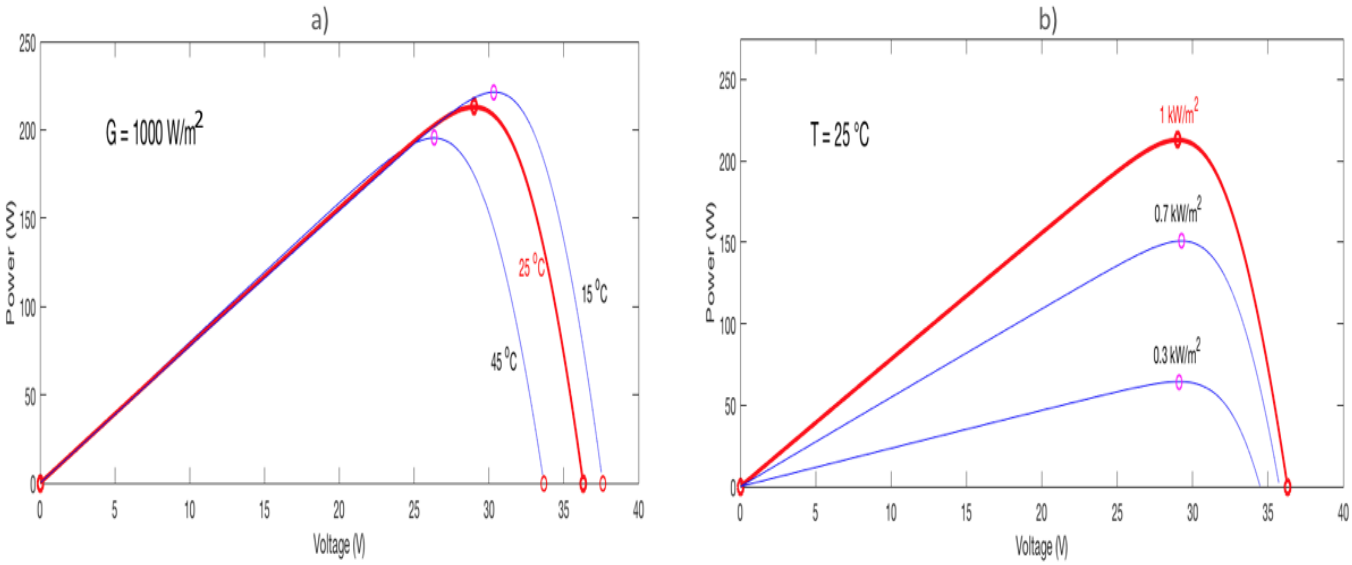

Figure 2.5: P-V curves of a PV module, plotted at: a) different temperature levels at $1000W/m^2$; b) different solar irradiance levels at 25°C.

For this purpose, Maximum Power Point Tracking (MPPT) techniques are required, in order to avoid power losses by varying the PV terminal voltage. MPPT techniques will be detailed in the next chapter.

2.5 Shading effects in PV module

Shading a solar module is equivalent to introducing a clog (impediment) in a pipe of liquid. The clog inside the pipe restricts the stream of water through the pipe. Identically, when a solar module is shaded, automatically the current flowing through the whole string is reduced.

Partial shading is one of the most causes that reduce the PV systems efficiency, approximately by 50% [31][32]. It happens due to several external influences such as neighbouring buildings, the existence of clouds, trees and snow.... The influence of

shadow differs depending on the string configuration, number of cells per module (36, 60 or 72 cells), the number of the bypass diode (BPD) and its placement. Figure 2.6.a shows a visual representation of the PV module configuration used in this study. In this case, the PV panel containing 60 cells is subdivided into 3 sub-strings or groups of cells of 20 cells each, and three bypass diode. A BPD does not prevent a cell to dissipate energy because it has to operate in the inverse bias in order to surmount the positive bias in the chain and activate BPD. Once a BPD is activated, it would provide an alternative path for the flow of current from the other strings as shown in Fig 2.6.b, but this means that a shaded cell may reduce the power of a conventional module by one third (60 cells, three BPDs). In the absence of a BPD, the power loss could be even greater [33].

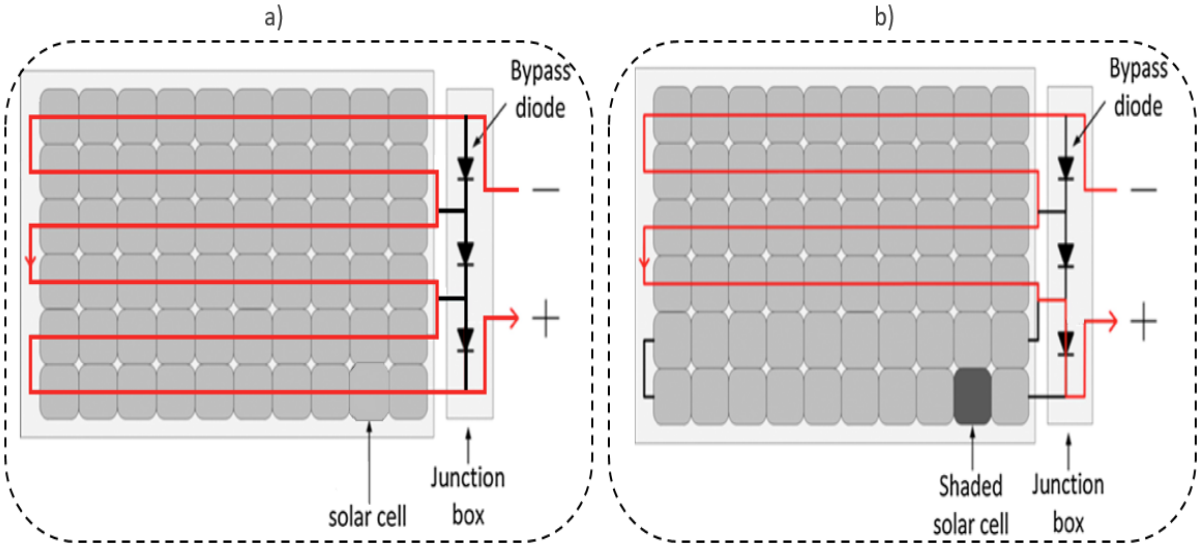

Figure 2.6: a) Schematic back side of a PV module with 60 solar cells; b) PV module with one shaded solar cell.

In this context, the PV string receives different value of irradiance, this effect generates a current mismatching, making the shaded cells to proceed as a resistor. In addition to that, instead of one MPP (unique peak), several local maximums appear which makes it difficult to differentiate between the local maximum power point (LMPP) and the global maximum power point (GMPP), which causes losses in the PV output power as it is described in Fig. 2.7 [34].

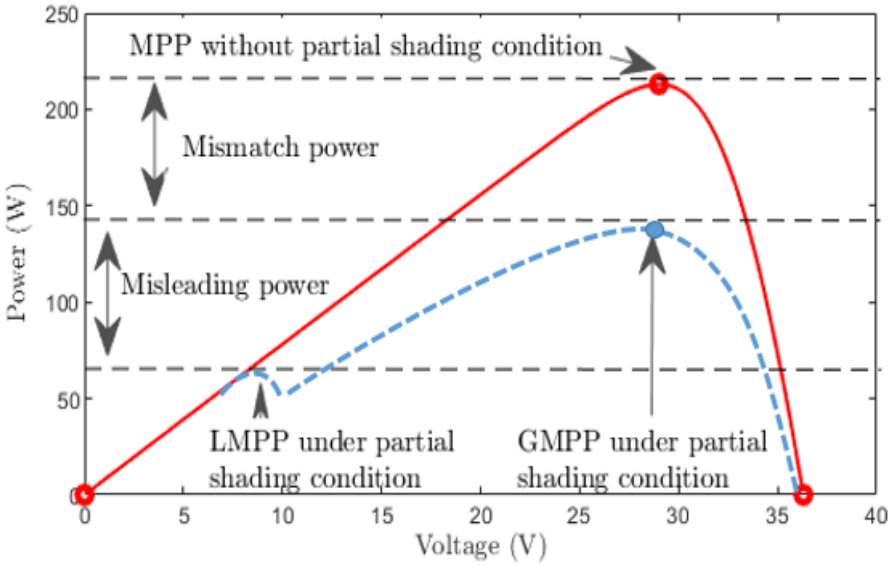

Figure 2.7: Representation of the different losses due to partial shading in a PV system.

Additionally, the output of the entire module may be greatly affected by the orientation of the shadow, where a horizontal orientation has a greater impact since it affects the whole cells of the module [35].

Approaches to Avoid shading drawbacks

In real application, the possibility of completely avoiding all the effects of partial shading remains a hard task. To mitigate these losses, engineering approaches have been developed [36], including the following solutions:

- PV module configurations;
- PV array configurations;
- Module Level Power Electronics (MLPEs).

2.6 Types of solar power systems

Photovoltaic solar systems include devices and equipment such as photovoltaic modules, charge controllers, inverters, battery bank.... Their design and cost estimation depends on the installation site, the building design, the required load profile and the type of solar module. Depending on the application and usage, they can be classified into two main categories, as stand-alone systems or grid connected PV systems [37].

Stand-alone systems, also called also called autonomous systems, are designed for regions where the utility grid is not available, such as isolated (remote) regions where the energy needed is limited and the solar source is available. Figure 2.8 presents the off-grid PV system components based block diagram [38].

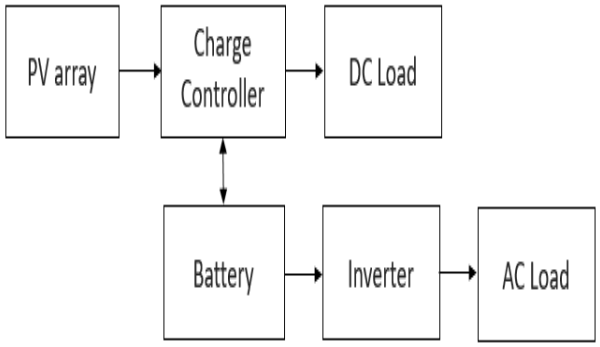

Figure 2.8: Off-grid PV system component based block diagram.

In case of grid-connected systems, DC electricity produced by the solar modules flows through a grid-connected inverter and is converted into AC electricity, which can be used by domestic electrical appliances or fed directly into the utility grid via a net meter or a bi-directional meter. Figure 2.9 presents the grid connected PV system component based block diagram [38].

In stand-alone systems, the PV string is usually over-sized to be able to store energy that can be used later, when solar irradiance is not available. In these systems, during sunny days, it may be not possible to use the maximum power available, especially

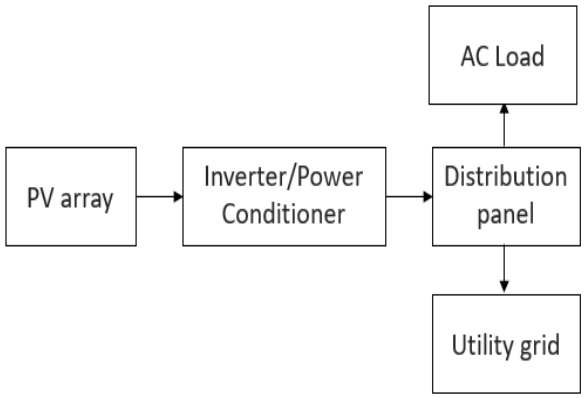

Figure 2.9: Grid connected PV system component based block diagram.

when the batteries are charged and consumption is low. In these situations, the MPPT algorithms are not relevant since the system can not operate at the MPP. Furthermore, an excessive oversizing may affect the MPPT controller [39]. In grid-connected PV systems, the maximum power is permanently extracted using the MPPT controllers and injected directly to the utility grid.

Chapter 3

Maximum power point tracking techniques

3.1 Introduction

External influencers such as temperature and solar irradiance introduce a non-linear characteristic to the system (see section 2.4). Furthermore, internal degradation and shadows may affect the system efficiency by introducing additional local maximums in the P-V curve (see section 2.5). These factors hinder the system to operate on its maximum power point (MPP), which affect the system efficiency.

In order to track the MPP continuously even when the atmospheric conditions change, the PV output voltage must be continuously adjusted towards its optimum value, this is called the Maximum Power Point Tracking (MPPT).

In this chapter, an overview of the MPPT algorithms is presented, attached with a detailed functional principle of three different MPPT algorithms, which are the Perturbation and Observation ($P\&O$), Particle swarm optimisation (PSO) and the Kalman filter (KF).

3.2 Overview about MPPT

In literature, there are about 10 different main MPPT techniques [10], and a dozens of variants have been investigated [40]. Each technique vary in tracking efficiency, convergence speed, complexity, number of sensors required and type of implementation hardware. Sumathi and Kumar [41] classified the MPPT techniques into three categories:

- **Off-line techniques** such as fractional short-circuit current (FSCC) and fractional open-circuit voltage (FOCV) techniques;
- **On-line or hill-climbing (HC) techniques** such as incremental conductance (InCond) and perturb and observe techniques;
- **Artificial-Intelligent (AI) techniques** such as artificial neural network (ANN) technique, fuzzy logic control (FLC) technique, particle swarm optimization (PSO) technique and genetic algorithm (GA).

Three different MPPTs are detailed and evaluated in the next section in order to analyse their performance in real test conditions.

3.3 Perturbation and Observation

Perturbation and observation ($P\&O$) technique is widely used and the most known MPPT algorithm since it is the simplest method among all MPPTs [42]. In addition to that, only two sensors are required to measure the PV's terminal voltage and current where the instantaneous power can be calculated.

The algorithm introduces a perturbation on one of the converter input parameters usually the PV output voltage V_{pv} by a constant value (ΔV). Right after, it observes the impact of this perturbation on the PV output power. According to Fig. 3.1, on the left side of the maximum power point, incrementing the voltage value is followed by an increase of the PV output power, whereas on the right side, incrementing the voltage

value is followed by a decrease in power. Based on this analysis, the *P&O* flowchart can be summarized in Fig. 3.2.

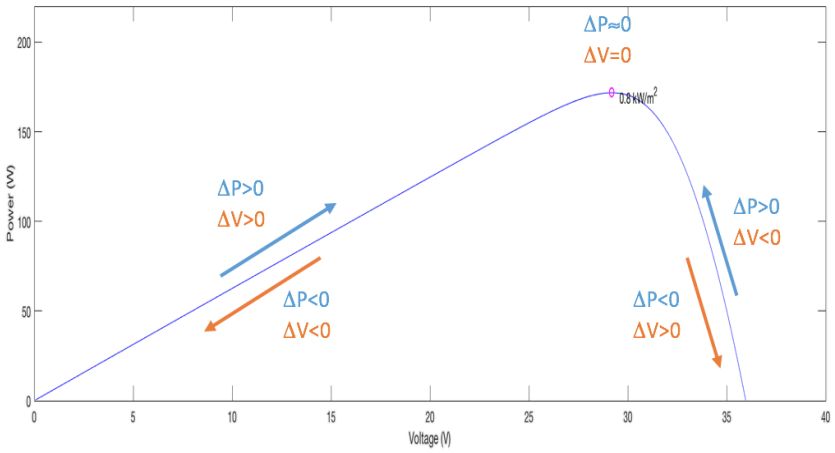

Figure 3.1: Operating principle of the P&O in the P-V curve.

The algorithm uses the PV voltage and current to calculate the PV output power. If the power variation increases ($\Delta P > 0$), the perturbation will continue in the same direction. Otherwise, the direction of the perturbation will be inversed, due to power reduction ($\Delta P < 0$) [43].

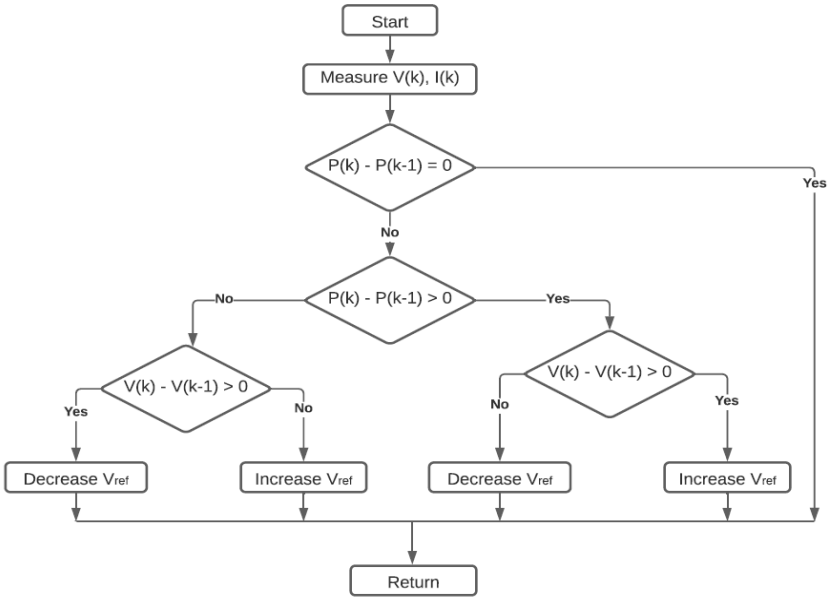

Figure 3.2: Flowchart of the MPPT based P&O technique.

The operating voltage is disturbed at every perturbation cycle, even when the MPP is achieved, which makes the power oscillates around the maximum operating point (MPP). These oscillations cause loss in the PV output power, and may affect the efficiency of the technique [44]. knowing that the amount of oscillation depends on the step width of the perturbation, two scenarios are possible:

- If the step width of the perturbation is large, more oscillation amplitude around the MPP occurs. However, the dynamic to achieve the MPP increases, even in fast changes of the atmospheric conditions.

- If the step width of the perturbation is small, less oscillation amplitude around the MPP occurs. However, the dynamic to achieve the MPP decreases.

In this work, the ideal step size of the perturbation is defined in the experimental part. Several works have been carried out to address this problem by setting a variable pitch during the maximum point search phase and the steady state phase around the MPP [45].

This technique presents an important drawback in rapid irradiance changes as Fig. 3.3 shows. At this stage, the system is disturbed towards the point C by the sunlight and not by the perturbation of the algorithm, which distances the search for the MPP from the operating point.

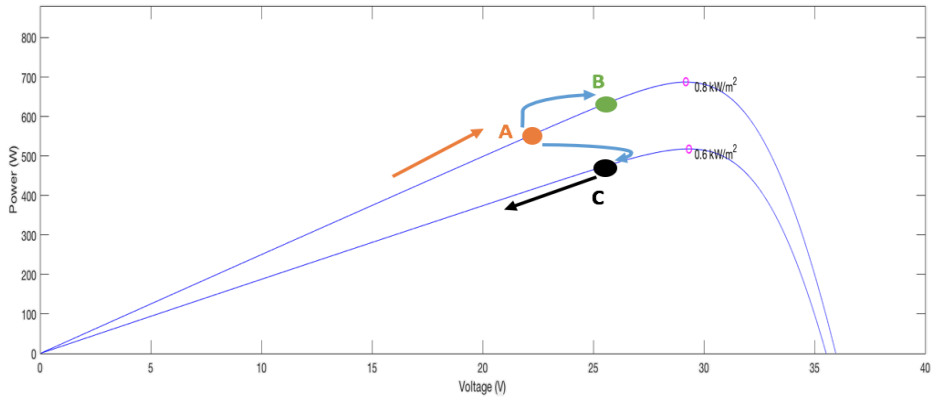

Figure 3.3: Wrong tracking of the P&O technique under sudden solar irradiance changes.

3.4 Particle Swarm Optimisation

3.4.1 Overview about the PSO

PSO algorithm was created in 1995 by Kennedy and Eberhart [46]. It was inspired by the social behaviour of animals evolving in swarms (example: Bird flocks), where each individual animal has a limited knowledge (local knowledge) about his situation in the whole swarm. The PSO technique plays a key role in solving wide optimization problems such as:

- Nonlinear problems;
- Multi-objective optimization;
- Unconstrained and constrained optimization problems.

3.4.2 Operating principal

The particle swarm is a group of simple agents called particles. Each particle is considered as a solution of the problem referred by a particular position x_i and velocity v_i. Additionally, each particle has two values to communicate with the other particles, where the first is the personal best performance p_{op-i} reached by the particle i, and the second is the global best p_{op-g}, which represents the optimal solution of all the particles [47].
Figure 3.4 presents the three components that control the movement of particles, which are:

- **Inertia weight component:** each particle has to follow its own current direction of shifting;
- **A cognitive component:** each particle has to follow the best location where it has already passed p_{po-i};
- **A social component:** each particle has to move towards the best location p_{po-g} already reached by the rest of the particles based on the shifting of its congeners.

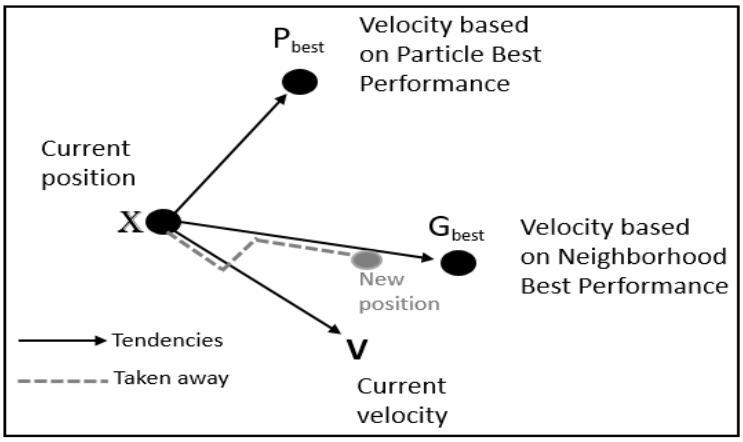

Figure 3.4: Particle movement in the optimization process.

Based on the shifting components, Eq. (3.1) shows the new position at iteration (t+1) adjusted by the PSO technique.

$$x_i(t+1) = x_i(t) + v_i(t+1) \quad , \quad i \in \{1, ..., n_i\} \tag{3.1}$$

Knowing that:

$$v_i(t+1) = wv_i(t) + c_1 r_1(p_{po-i} - x_i(t)) + c_2 r_2(p_{po-g} - x_i(t)) \tag{3.2}$$

Where:

i: The index of the particle;

n_i: Number of particles;

$x_i(t)$: The position of the particle i at the instant (t);

$x_i(t+1)$: The position of the particle i at the instant (t+1);

$v_i(t)$: The shifting of the particle i at the instant (t);

$v_i(t+1)$: The shifting (velocity) of the particle i at the instant (t+1);

w: Coefficient of inertia;

c_1 and c_2: Acceleration coefficients;

r_1 and r_2: Two random values drawn uniformly between zero and one;

p_{op-i}: The best position of the particle i;

p_{op-g}: The best position of all the particles of the swarm.

The performance evaluation of the swarm particles is done by a maximum character function, called fitness function (F). In order to improve the performance of the particles (position and velocity), a comparison at every iteration using the fitness function is done between the current position and the best local position to define the new local best p_{po-i}, and also between the current position and the global best position to define p_{po-g}, which can be summarized in the following equations [48].

$$if \quad F(x_i(t+1)) > F(p_{op-i}) \Rightarrow p_{op-i} = x_i(t+1) \tag{3.3}$$

by the same:

$$if \quad F(x_i(t+1)) > F(p_{op-g}) \Rightarrow p_{op-g} = x_i(t+1) \tag{3.4}$$

3.4.3 PSO based MPPT process

The analogical adaptation of the PSO technique in the instantaneous search of the MPP is based on considering the position of the particle (x_i) analogous to the duty cycle D_i, which represents the DC / DC boost converter control signal. Likewise, the shifting speed (v_i) is analogous to the variation in duty cycle at every iteration (ΔD_i), while the fitness function is defined as the PV output power corresponding to the duty cycle of each particle [48][17]. In summary:

$$\begin{cases} x_i(t) & \equiv & D_i(t) \\ v_i(t) & \equiv & \Delta D_i(t) \\ p_{op-i} & \equiv & d_{op-i} \\ p_{op-g} & \equiv & d_{op-g} \\ F(x_i) & \equiv & P(D_i) \end{cases} \tag{3.5}$$

Where Eq. (3.1) and Eq. (3.2) become :

$$D_i(t+1) = D_i(t) + \Delta D_i(t+1) \quad , \quad i \in \{1, ..., n_i\} \tag{3.6}$$

Knowing that:

$$\Delta D_i(t+1) = w\Delta D_i(t) + c_1 r_1 (D_{op-i} - D_i(t)) + c_2 r_2 (D_{op-g} - D_i(t)) \tag{3.7}$$

Where:

$D_i(t)$: The duty cycle of the particle i at the instant (t);

$\Delta D_i(t)$: The variation of the duty cycle of the particle i at the instant (t);

D_{op-i}: The best duty cycle of the particle i;

D_{op-g}: The best duty cycle of all the particles of the swarm.

Using the fitness function at every iteration, the PSO defines the corresponding power of the duty cycle of each particle in the swarm, where the best local power of each particle and the global best power are updated by comparison using Eq. (3.8) and Eq. (3.9), respectively, according to their duty cycles [49].

$$if \quad P(d_i(t+1)) > P(d_{op-i}) \Rightarrow d_{op-i} = d_i(t+1) \tag{3.8}$$

by the same:

$$if \quad P(d_i(t+1)) > P(d_{op-g}) \Rightarrow d_{op-g} = d_i(t+1) \tag{3.9}$$

Figure 3.5 shows the flowchart of the PSO based MPPT technique [50], which can be described in the following steps:

- Step 1: This step includes the initial number of particles n_p all over the space research, attached with their initial duty cycles and velocities.

  The choice of the parameters w, c_1 and c_2 have an essential importance in the optimisation process. Regarding the social component c_2 and the cognitive component c_1, a large value of c_2 compared with c_1 make the optimization biased towards the

global best recovery p_{op-g}. Otherwise, the sampling related to the local best p_{op-i} will be preferred. Plenty of research in literature improves the variance of these values as a variable function for better exploitation and the exploration [48].

- Step 2: Calculate the fitness value of each particle by sending the particle solution to the fitness function (objective function)..
- Step 3: Update the best individual positions p_{op-i} of each particle and the best overall fitness value p_{op-g} using Eq. (3.8) and Eq.(3.9), and replace the corresponding p_{op-i} and p_{op-g} at their position if necessary.
- Step 4: If all particles are evaluated, update the velocity ΔD_i and duty cycle D_i of all the particles using Eq. (3.7) and Eq. (3.6), respectively. Otherwise, repeat step 2 through step 4.

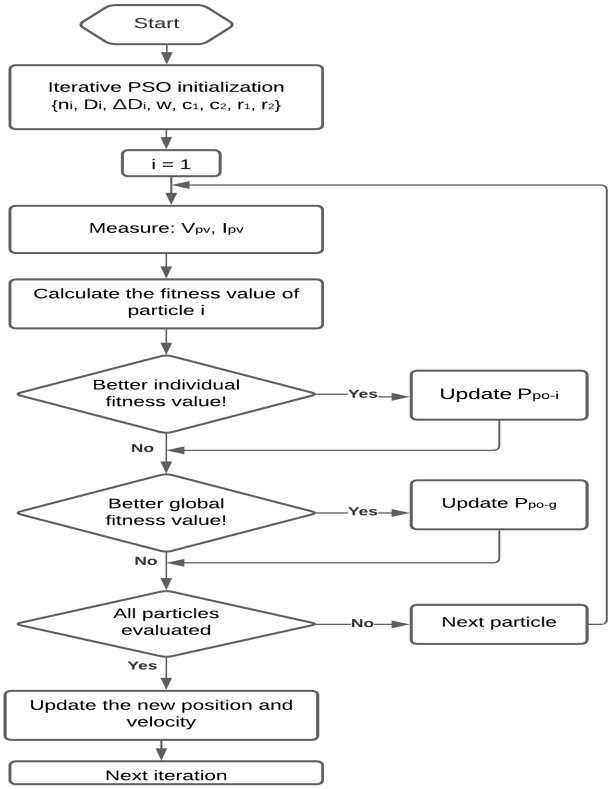

Figure 3.5: Flowchart of the MPPT based PSO technique.

3.5 Kalman filter

3.5.1 Overview about the Kalman filter

Kalman filtering is an optimal estimation approach that has been widely implemented in real-time computational dynamics. The Kalman filter estimates the state of a dynamic systems based on two different models, a dynamic model and an observation model. The dynamic model defines the behaviour of the state vector, while the observational model sets out the relationship between the state vector and the measurement [15]. Both models are equipped with statistical features to describe the accuracy of the models following Fig 3.6 [51]. In many applications, the statistical noise levels of the model are provided before the filtering process and remain unchanged during the recursive process. Usually, this priori statistical information is determined by trial analysis and some prior knowledge about the type of observation. If this priori information is insufficient to represent the real statistic noise level, the Kalman estimate is not optimal and can lead to unreliable results, sometimes even filtering out discrepancies [15][52]. Reference [15] offers an adaptive filter which can retrieve the appropriate noise covariances and can enhance the filter performance to deal with data assimilation problems.

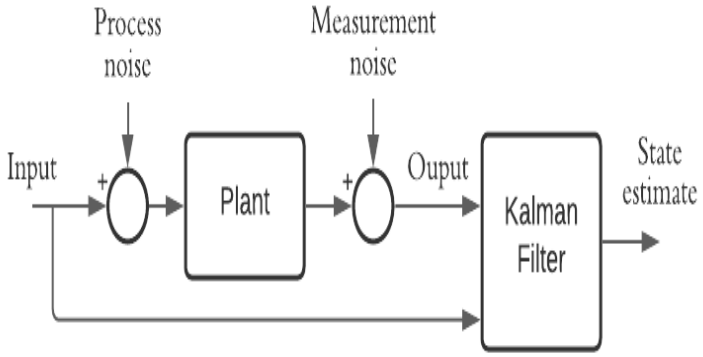

Figure 3.6: Generic block diagram to illustrate the Kalman filter technique.

Nowadays, Kalman filter is widely used in several applications such as [53]:

- Medical and Biological Sciences.
- Tracking and Positioning such as GPS systems.
- Electrical Engineering.
- Industrial Applications and Communications.

3.5.2 Kalman filter principle

The KF technique is an iterative mathematical process that uses a set of equations and consecutive data inputs to quickly estimate the actual values (velocity, position, etc...) of the object being measured. The KF technique supports estimations of the state across the entire time axis (past, present and future) especially when the measured values contain unpredicted random errors, or the nature of the modeled system is not known [12].
The KF algorithm combines periodically the inputs from the observation state (physical measurement) with the prediction state (predicted by the algorithm) of a particular situation. Furthermore, the different errors and uncertainties of the process noise and the measurement noise are taken into consideration by using a stochastic state-space representation, in order to reduce the imperfections of the controlled state [54][55].

The set of equations of the KF technique is divided in two groups [54]. Firstly, the predicted equations (the time update), which are:

$$X^p_{act}(k) = AX_{act}(k-1) + Bu(k-1) + w(k-1) \tag{3.10}$$

$$P^p(k) = AP(k-1) + Q \tag{3.11}$$

The first equation represents the state vector predicted by the algorithm, where $X^p_{act}(k)$ is the prediction of the actual state vector at iteration k given by the results of the previous iterations, $X_{act}(k)$ is the actual state vector estimation at iteration $k-1$ adjusted by a

physical measurement, u is the control variable matrix, which refers to the input system [17], A and B are constant matrices used to adapt the system to the KF process, w refers to the imperfections of the modeling process [55].
The second equation, $P^p(k)$ represents the priori process covariance matrix (the error in the estimate), and Q is the process noise covariance matrix which tends to keep the process covariance matrix from becoming too small or tends to zero. When the imperfections of the modeling process is known, the process noise covariance can be calculated as [51]:

$$\mathcal{E}\{w(k) \times w^T(k)\} = \begin{cases} Q(k) & \textbf{if } i = k \\ 0 & \textbf{if } i \neq k \end{cases}$$

Secondly, the corrector equations (the measurement updates) consist of three equations, where the main role is to adjust the predicted state vector and process covariance by using data from the physical model. The Kalman gain is calculated at first using Eq. (3.12).

$$K(k) = \frac{P^p(k)H}{HP^p(k)H^T + R} \tag{3.12}$$

Where, $P^p(k)$ is the priori process covariance matrix calculated in Eq. (3.11), H is a constant which depends on the concerned system in which the KF technique is applied, and R is the output measurement error covariance matrix based on the the space-vector representation of the Kalman filter model. If the measurement noise $z(k)$ is completely known, the measurement error covariance can be calculated as follows [51]:

$$\mathcal{E}\{z(k) \times z^T(k)\} = \begin{cases} R(k) & \textbf{if } i = k \\ 0 & \textbf{if } i \neq k \end{cases}$$

The Kalman gain is called also the weight factor, and it compares the error in the estimate with the error in the measurement. If R is higher than $P^p(k)$, i.e. the measurement update includes more uncertainties compared to the predicted update. Therefore, the Kalman gain must tend to 0, considering the predicted state as a confident update, and vice versa.

The second equation refers to update the adjusted state vector $X_{act}(k)$ by combining the measured voltage given by sensors Y_{meas} and the measurement output given by the KF model $Y^p(k)$ following Eq. (3.13).

$$X_{act}(k) = X^p_{act}(k) + K(k)\left(Y_{meas}(k) - HY^p(k)\right) \tag{3.13}$$

Knowing that the measurement output equation depends on $X_{act}(k)$ and the measurement noise $z(k)$, which can be written following as:

$$Y^p(k) = CX_{act}(k) + z(k) \tag{3.14}$$

The last equation updated is the posterior process covariance $P(k)$ given by the following equation:

$$P(k) = (I - k(k)H)\,P^p(k) \tag{3.15}$$

Where I is the identity matrix, and $P^p(k)$ is the priori process covariance at the same iteration as the posterior process covariance.

3.5.3 Kalman filter based MPPT process

To achieve the tracking of the maximum power point, the position of the operating point must be projected continuously. According to the P-V characteristic of the PV array shown in Fig. (3.1), the curve represents a convex function where the PV power increase with a positive slope $\frac{\Delta P}{\Delta V}$ until achieve the MPP, right after the optimal point power decreases with a negative narrow slope. On the other hand, the state vector of the KF based MPPT is composed by only one state variable which is the PV string output voltage reference imposing A equal to 1. Based on this features, a similar one dimension linear state space equation can be formed, where the MPPT can be governed by the following equation [51]:

$$V_{ref}^{p}(k) = V_{ref}(k-1) + B\frac{\Delta P}{\Delta V}(k-1) + w \tag{3.16}$$

Where $V_{ref}^{p}(k)$ is the voltage reference predicted by the MPPT controller at iteration k, $V_{ref}(k-1)$ is the voltage reference corrected (step-up input voltage reference) at iteration $k-1$ based on physical measurement, B refers to the scaling factor (step size), $\frac{\Delta P}{\Delta V}$ is the instantaneous power slope which reflects the control variable matrix. w presents the mix of disturbances of the design, such as the switching noise generated by switching devices, the thermal noise and also the electro-magnetic interference. Even without the errors between the PV array and the power electronic device, there are some other errors caused by the voltage and current sensors in order to recover the measured slope $\frac{\Delta P}{\Delta V}$ [13][17]. In this work, the measured voltage $V_{meas}(k)$ follows the Eq. (3.17):

$$V_{meas}(k) = V_{ref}(k) + z \tag{3.17}$$

Where z is the error (uncertainties) between V_{meas} and V_{ref} at the same iteration, as it is described in Fig. 3.7, in which the noises are supposed to be white Gaussian and uncorrelated each other [54].

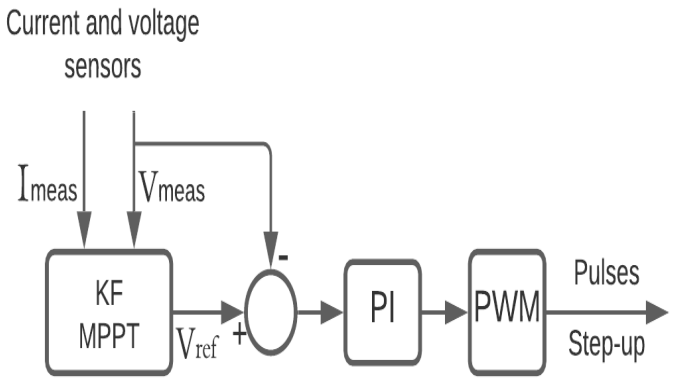

Figure 3.7: Controlling errors between the measured voltage and the reference voltage [17].

Two known values, $V_{meas}(k)$ and $\frac{\Delta P(k)}{\Delta V(k)}$ are used for the KF based MPPT, which leads to describe the flowchart (Fig. 3.8) in the following steps:

- Step 1: update the predicted voltage reference

$$V_{ref}^{p}(k) = V_{ref}(k-1) + M\frac{\Delta P}{\Delta V}(k-1) \tag{3.18}$$

  In real systems, the amount of noises is important especially the slope $\frac{\Delta P}{\Delta V}$ since it is more sensitive. Therefore the predicted results can present failures in tracking the MPP. The slope can achieve an unexpected magnitude around 10^5 (observed experimentally) due to noise. This situation has occurred when the voltage variation (ΔV) becomes infinitesimal. In this work, a protection block is implemented experimentally in order to avoid this drawback.

- Step 2: update the priori process covariance (error in estimate), where Q refers to the process noise covariance between the priori and the posteriori process covariance, it imposes a tradeoff between the dynamicity and the stability of the tracking process around the MPP. In this work, by fixing the measurement error R (appendix A), the process noise covariance can be tuned by trial process.

- Step 3: update the kalman gain by using the measurement noise covariance R and the priori process covariance $P^p(k)$, which in turn requires the process noise covariance value Q [17].

- Step 4: update the corrected voltage reference (step-up input voltage reference) V_{ref} by controlling the error between the predicted voltage reference V_{ref}^{p} and the measurement input given by the voltage sensor in Eq. (3.17), using the kalman gain given by Eq. (3.12).

- Step 5: update the posteriori process covariance $P(k)$ using Eq. (3.15). As the number of iterations progresses, $P(k)$ will be smaller and tends to zero. Thus, the noise will be gradually eliminated from the final estimations [51][14].

At this stage, it should be clear that the KF technique suggests also a process that reduces the noise effects in the tracking computation [54].

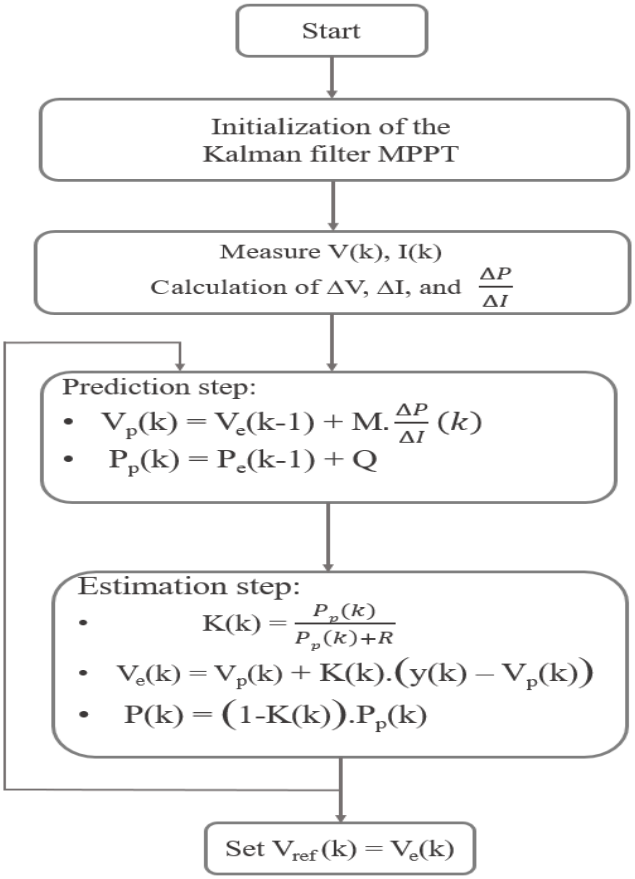

Figure 3.8: Flowchart of the MPPT based KF technique.

Chapter 4

Experimental setup and implementation

Introduction

In order to validate the theoretical description of the previous chapter, experimental tests were carried out on real grid-connected PV system. The experiments were carried out in the LSE laboratory (Electro Mechatronics Systems Laboratory, Instituto Politécnico de Bragança, Portugal).

This chapter focus on the power topology used during this work, attached with the electrical characteristics of the static material used. This chapter provides also a description on the implementation of the algorithms evaluated, using a duality of *MATLAB/Simulink* software and *dSPACE* 1103 *real time controller board*.

4.1 Power Structure

Figure 4.1 illustrates the power structure used for the experimental tests. It is composed of PV string connected to a PM75RLA120 intelligent power module (IPM) from Powerex, which provides a three-phase IGBT inverter. The first arm (U) operates as a boost converter by maintaining the upper IGBT (switch 1) continually OFF. While the other

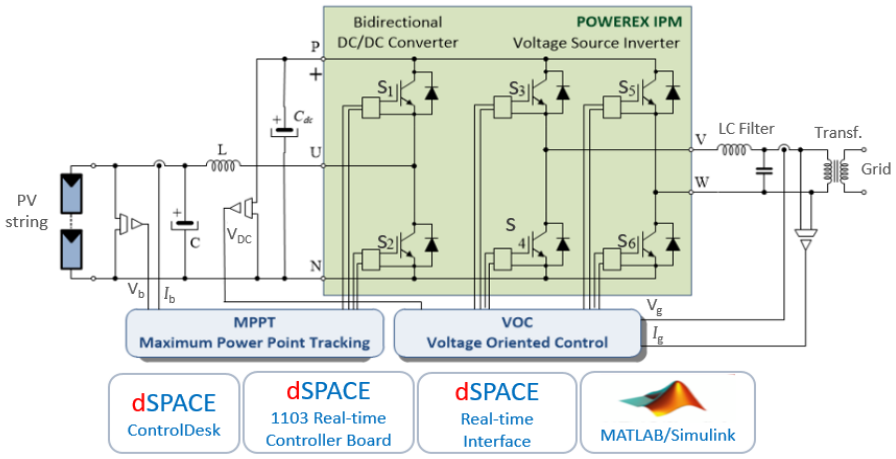

Figure 4.1: System power structure.

arms (V and W) operate as a single phase voltage source inverter (VSI) [56]. An LC output filter is used, attached with an insulation transformer for protection purpose between the grid (active load) and this PV system.

Figure 4.2 shows the hardware setup, where the measurement module is a signal processing interface for data acquisition and filtering. While the dSPACE 1103 real-time board controls the single phase VSI and the boost converter based on the MPPT and VOC blocks, which are implemented in *Simulink* with *Real−Time Interface* and *ControlDesk*.

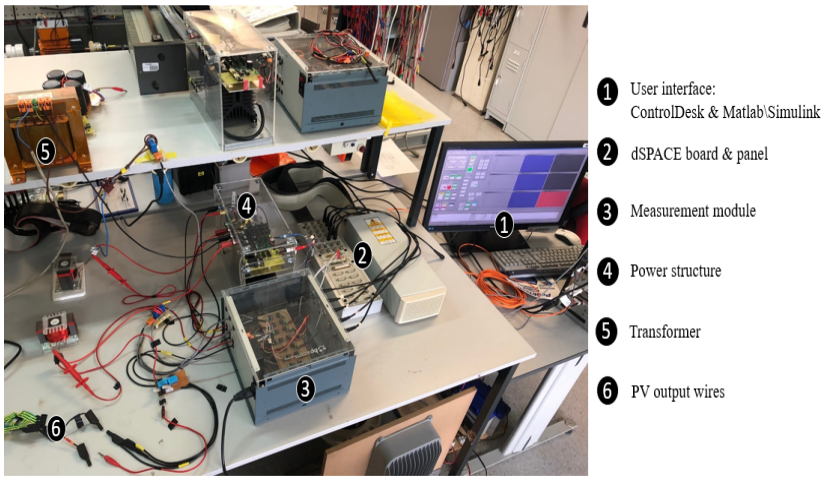

Figure 4.2: Hardware setup.

4.1.1 PV string

Figure 4.3 shows the two PV string models used for the experimental test presented in this work. The first string (string A) consists of 5 series-connected Fluitecnik FTS220P PV modules and is used for the tests under normal operating condition since it is installed on the roof the laboratory. While the second string (string B) consists of 3 REC 275PE PV modules also connected in series. it is used for the test under shadow effect (see section 2.7), since it is installed in front of the laboratory, which ease the implementation of the artificial shadow. Table 4.1 shows the electrical characteristics of PV models used.

Figure 4.3: PV string models.

Characteristics	P_{max}	V_{MPP}	I_{MPP}	V_{oc}	I_{sc}
Model A	220 W	29.38 V	7,51 A	36.76 V	8.30 A
Model B	275 W	31.5	8.74 A	38.7 V	9.25 A

Table 4.1: Electrical characteristics of the PV modules.

4.1.2 DC-DC converter

The DC/DC converter controls the output voltage of the PV string (input voltage of the converter) and limits the maximum output voltage (DC-link voltage) to an appropriate level. The DC-DC converter controller is designed to operate as an MPPT block, which

provide a PWM signal to control the switch (IGBT 2) of the converter. The values of the capacitor C_{dc} and the inductor L are 1000 μF and 12 mH, respectively.

4.1.3 DC-AC converter

A single phase Voltage Source Inverter (VSI) is applied to balance the power flow from DC bus to the grid. It consists of four IGBTs controlled using voltage oriented control (VOC), by providing the reference PWM. The VOC ensures the grid synchronization and the control of active power by keeping the DC-link voltage constant at $400V$. Figure 4.4 shows the block diagram of the VOC control, which is based on the transformation between a stationary frame ($\alpha\beta$) and a rotating frame (dq), in order to control the decoupled direct current separately using two PID controllers, where the control of the active and reactive is also possible [56][57], knowing that:

- A phase locked loop (PLL) is used to obtain a pure image of the grid voltage (providing the grid voltage amplitude and the angle (θ) between the stationary and rotating frames);
- The synchronous frame (dq) rotates at the angular speed of the grid space-vector (100π);
- The grid voltage space-vector is aligned with the direct component (d) of the rotating frame;
- The proportional and integration gains for the current component are set to be 20 and 2000, respectively, while that of the DC link voltage are set as 0,19 and 10.

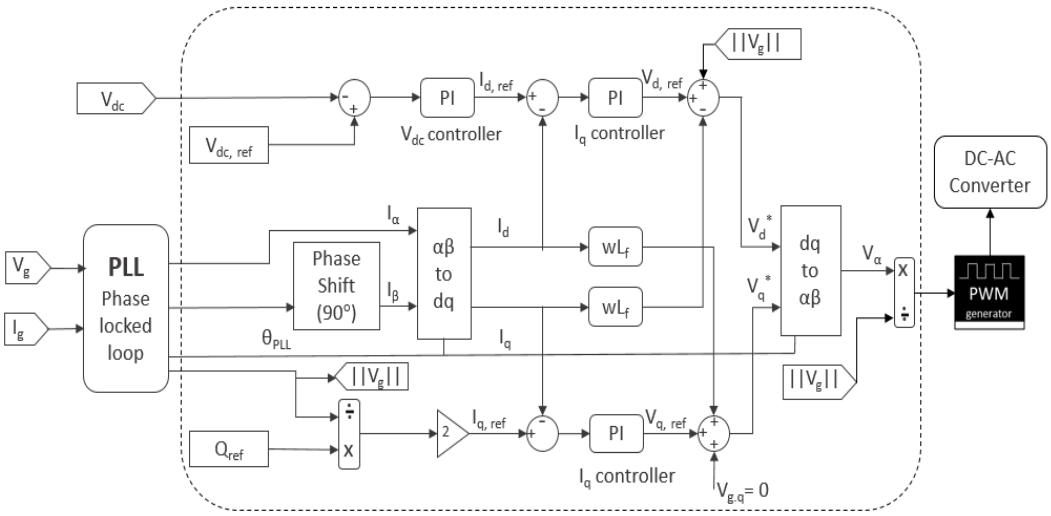

Figure 4.4: Block diagram of the Voltage Oriented Control.

4.2 Algorithms' implementation

Figure 4.5 shows the block diagram control where the three evaluated techniques operate. The *PSO* algorithm does not require any PI controller, since it generates directly the duty cycle for the IGBT of the boost converter. Unlike the *P&O* and *KF* techniques, which generate at first a reference voltage. Table 4.2 shows the proportional and integration gains used for the *P&O* and *KF* techniques.

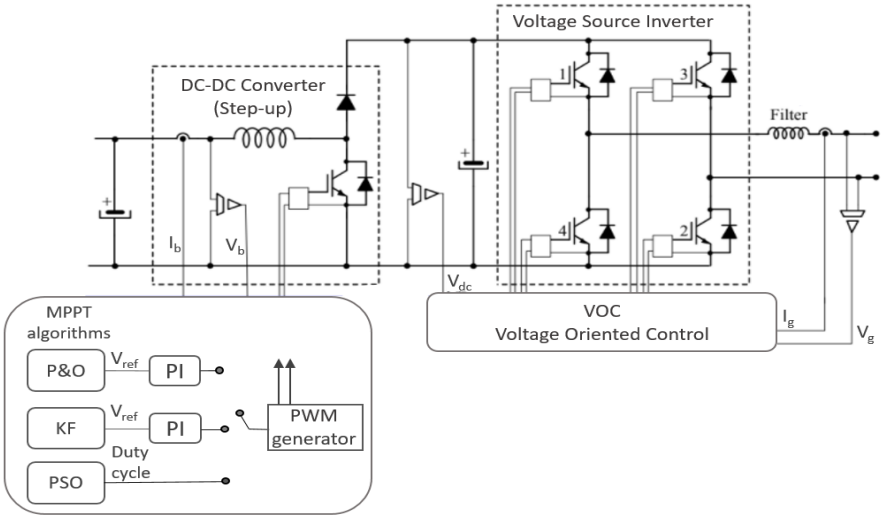

Figure 4.5: Power structure control configuration.

Gain	Value
Proportional gain (K_p)	20
Integration gain (K_i)	2000

Table 4.2: Gains of the PI controller used for $P\&O$ and KF techniques.

The implementation of the MPPTs block were carried out by using *Simulink* with $dSPACE$ 1103 $real-time\ controller\ board$, where the analogue measured quantities of the PV current and PV voltage are assigned to the A/D converter of the controller board, so as to be used by the *Simulink* MPPT control block. The output signal given by the MPPT control block is then applied towards the $DS1103SL\_DSP\_PWM$ block, in order to provide the switching signal used for driving the IGBT.
In order to proceed real time tracking of the MPP, the *Simulink* MPPT block must be downloaded on the dSPACE board, so as to generate a C code according to each MPPT control block.

4.2.1 Implementation of Perturbation and Observation technique

Figure 4.6 shows the *Simulink* MPPT block of the $P\&O$ technique, where the increment (perturbation) is chosen to be 4V.

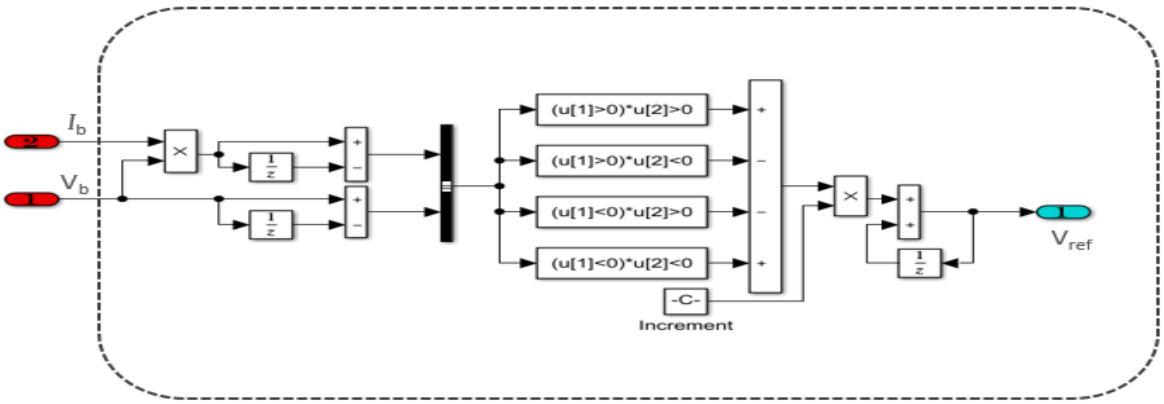

Figure 4.6: Simulink diagram of the P&O technique.

4.2.2 Implementation of Kalman Filter technique

Figure 4.7 shows the *Simulink* MPPT block of the KF technique, while Table 4.3 shows the required parametrization used in this work. A protection block is applied to avoid the divergence of the slope, when the measured PV voltage difference between two successive iterations ΔV becomes infinitesimal.

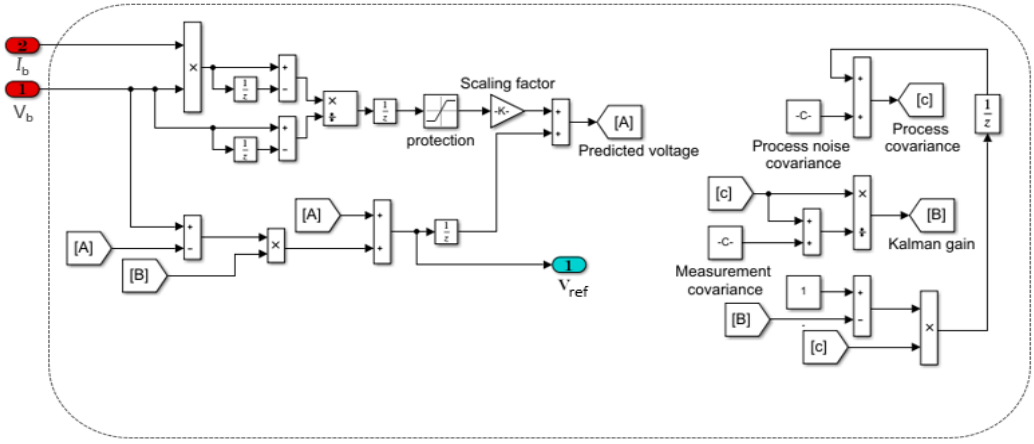

Figure 4.7: Simulink diagram of the KF technique.

Parameter	value
B	1
P_0	0
Q	0.265
R	0.405

Table 4.3: Parameterization of the KF technique.

The setting of measurement covariance R was carried out using the Excel program via a measurement signal, while the value of Q was set experimentally by tuning this value in real-time. The initial value of the process covariance P_0 is chosen to be 0 since the distance between the predicted voltage and the reference voltage is unknown.

4.2.3 Implementation of the PSO technique

Figure 4.8 shows the *Simulink* MPPT block of the PSO technique, while table 4.4 shows the required initial parametrization used in this work. The number of particles is chosen

to be 5 particles. It should be specified that a large number of initial particles may generates a large amount of oscillation at the beginning of the tracking.

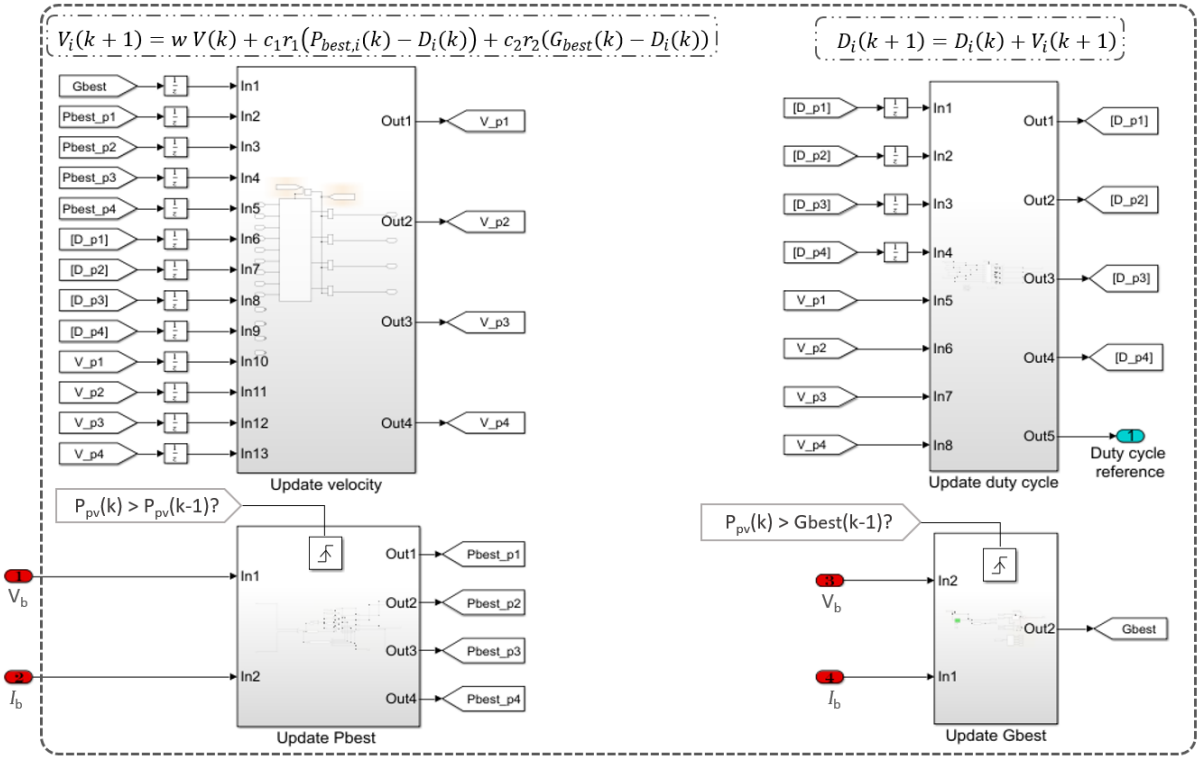

Figure 4.8: Simulink diagram of the PSO technique.

Parameter	value
n_p	5
w	0.4
c_1	1.2
c_2	2.2

Table 4.4: Parameterization of the PSO technique.

Chapter 5

Experimental results and discussion

This chapter is divided into two parts. The first presents the test protocol of the algorithms evaluated, attached to the experimental results carried out under two situations: under normal operating conditions, and under shadow conditions. The second part stands on the discussion regarding the tracking performance of each MPPT technique.

5.1 Experimental results

In order to compare experimentally the performances of the MPPTs evaluated, two sets of tests were curried out. Firstly, the tests under normal operating conditions, which were carried out in sunny day, where the irradiation and temperature are almost constant for the entire duration of the tests applied with the three algorithms. Figures 5.1 and 5.2 show the ambient atmospheric solar irradiance and temperature, where the tests are performed on 09/03/2021 between 11:20 pm and 12:50 pm. During the testing period, the ambient solar irradiance varies around 4% and the ambient temperature varies around 8%, which will not affect the performance comparison between the MPPTs evaluated. Secondly, the tests under partial shading conditions, where the purpose is to discover the capability to deal with shadow effect described in section 2.5.

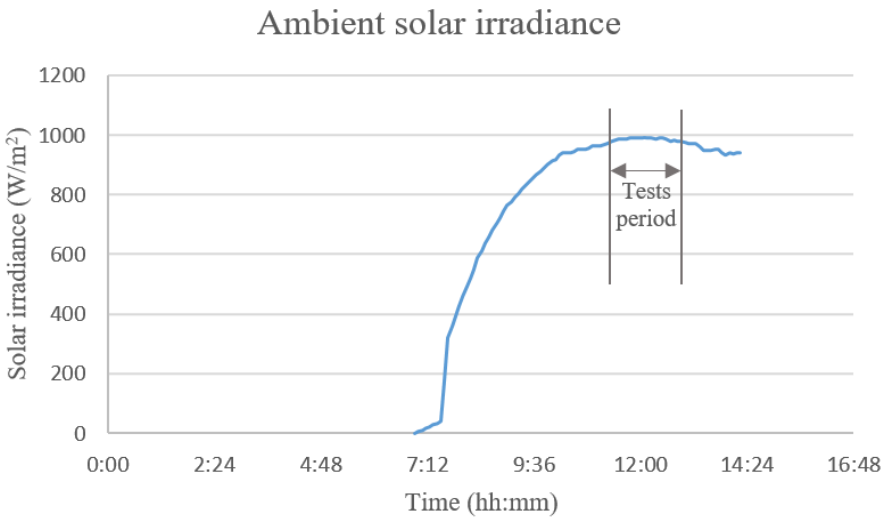

Figure 5.1: Ambient solar irradiance.

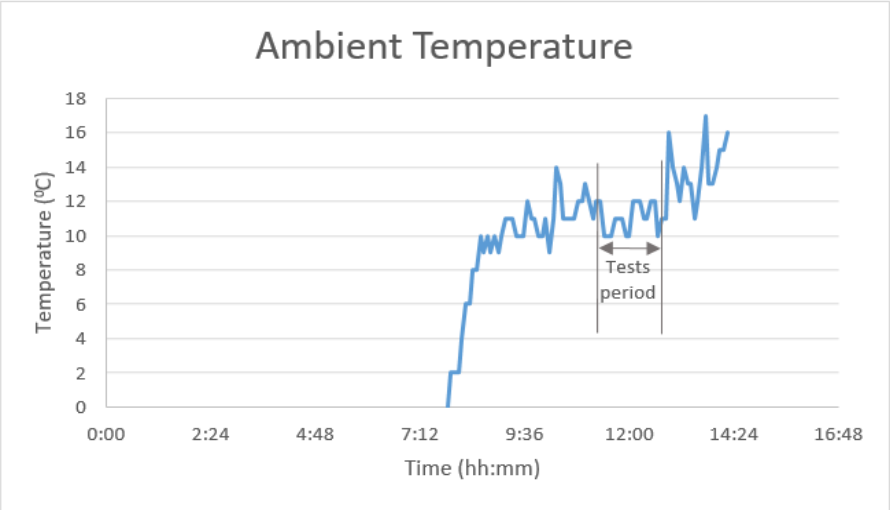

Figure 5.2: Ambient temperature.

Since the PV output voltage at the maximum power point V_{MPP} is located at around 0.8 of the open-circuit voltage V_{oc}, about 65% of the P-V curve (including the MPP) was traced by using a ramp block following Figs. 5.3 and 5.4.

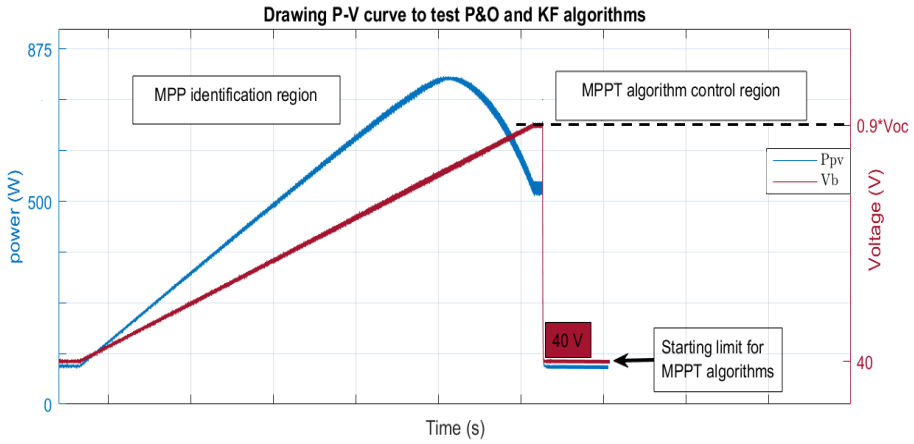

Figure 5.3: P-V curve identification for P&O and KF algorithms.

Figure 5.3 shows that the PV output voltage increases linearly from $40V$ to $0.9V_{oc}$, where the MPP is included. Thereafter, the $P\&O$ and KF techniques are launched after turning back the output PV voltage at $40V$.

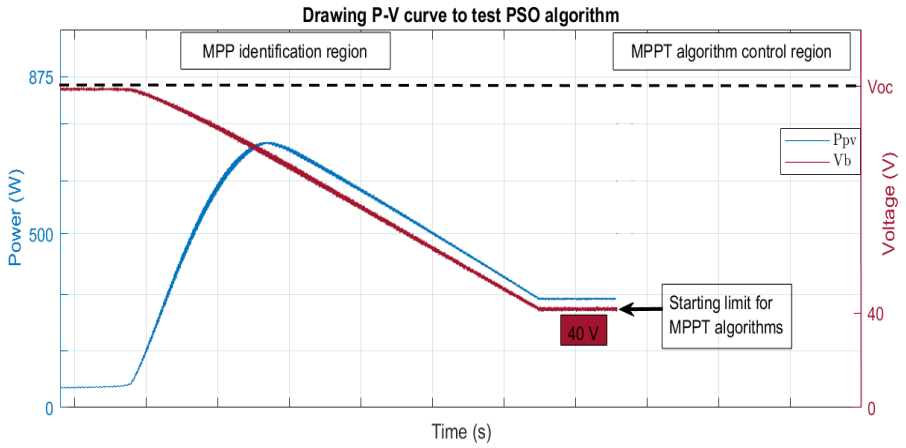

Figure 5.4: P-V curve identification for PSO algorithm.

Figure 5.4 shows that in the case of the PSO technique, the PV output voltage decreases linearly from the V_{oc} to $40V$, which is imposed by increasing linearly the duty cycle from 0.4 to 0.9. Thereafter, the PSO technique is launched at the same voltage value $40V$.

5.1.1 Tests under normal operating conditions

Tests under normal operating conditions are performed using the PV string A shown in Fig. 4.3, where the three MPPT techniques are executed with the same cadence at $0.1s$. Figures 5.5, 5.6 and 5.7 show the performance tracking of the MPPT techniques evaluated in this work.

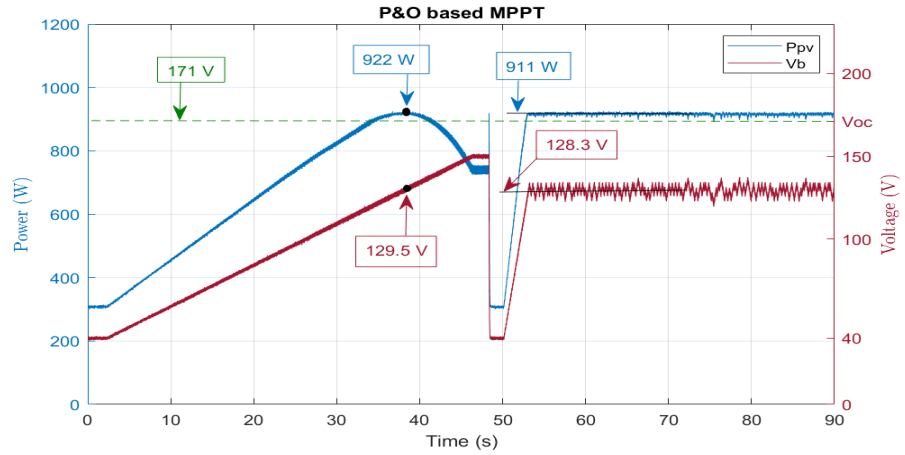

Figure 5.5: Test under normal operating conditions using P&O.

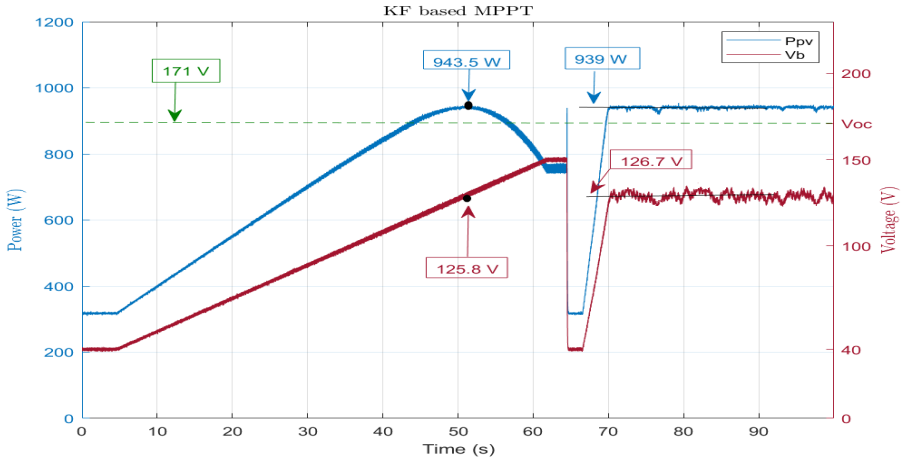

Figure 5.6: Test under normal operating conditions using KF.

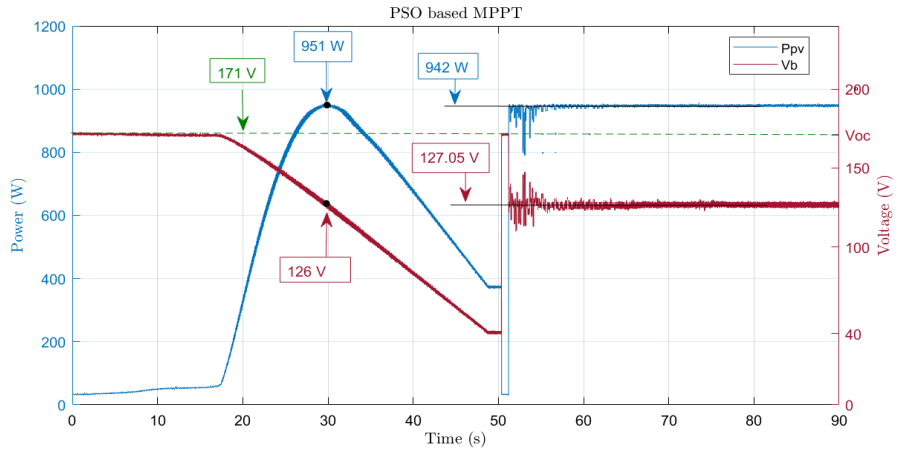

Figure 5.7: Test under normal operating conditions using PSO.

5.1.2 Tests under partial shadow conditions

Tests under shading are performed using the PV string B shown in Fig. 4.3. Where the purpose lies in the ability to operate around the global MPP described in section 2.5. The artificial shadow was realized using a semitransparent film on a small portion of string B as in Fig. 4.3. Figures 5.8, 5.9 and 5.10 show the performance tracking of the MPPT techniques evaluated under shading conditions.

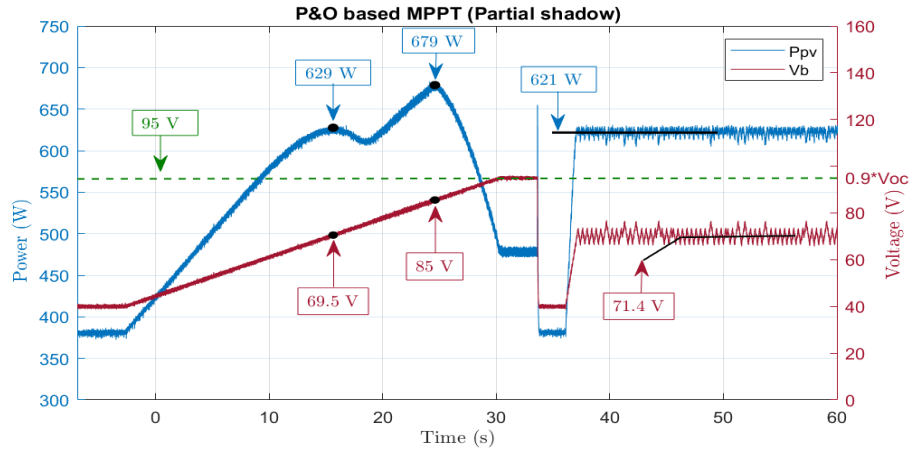

Figure 5.8: Test under partial shadow condition using P&O.

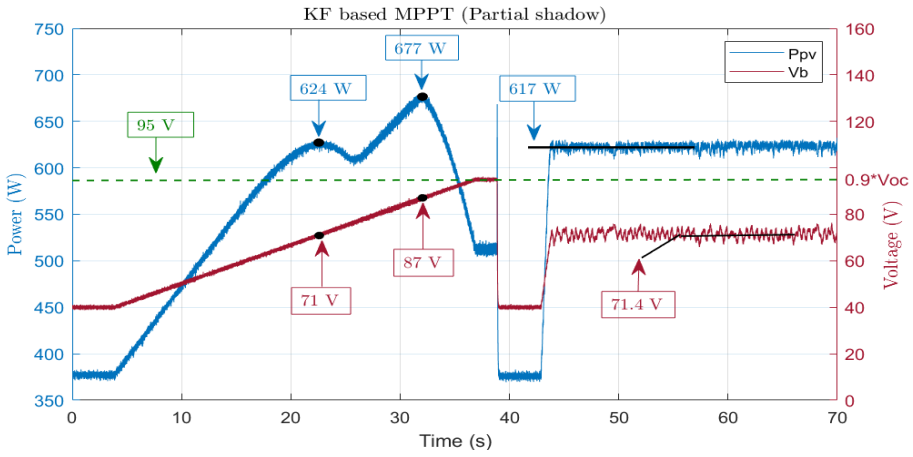

Figure 5.9: Test under partial shadow condition using KF.

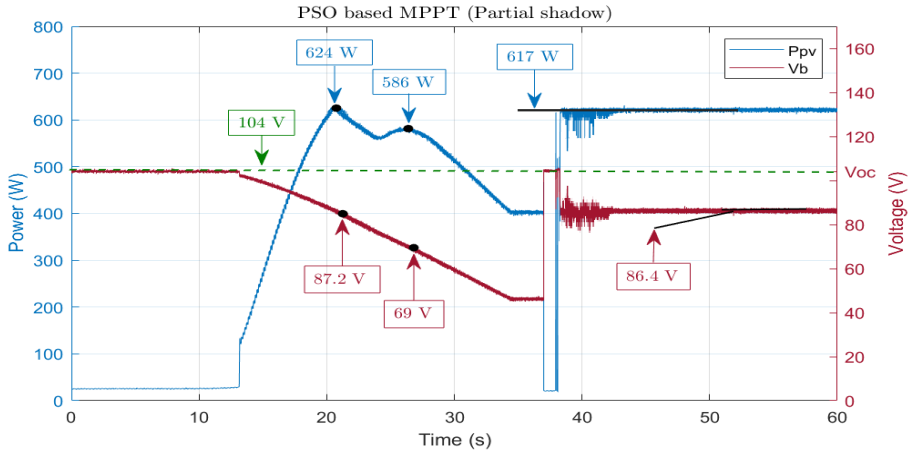

Figure 5.10: Test under partial shadow condition using PSO.

5.2 Discussion

The results obtained in Figs. 5.5, 5.6 and 5.7 share the same test conditions, such as the temperature, solar irradiance exposed, hardware setup and execution cadence of the algorithms, where their evaluation can be performed to compare the precision to reach the MPP, the oscillation around the MPP at steady state, the response time (speed convergence) and the ability to deal with partial shading conditions.

The aptitude to reach the MPP

The results in Fig. 5.5, 5.6 and 5.7 show that the P-V curve obtained by the ramp block includes a single MPP. The difference between the MPP and the operating point achieved by each MPPT technique represents the aptitude in reaching the MPP. In short, the algorithm which operates closer to the MPP extracts more power from the PV String. The aptitude to reach the MPP can be calculated using Eq. 5.1 and 5.2, where V_{MPP} is the voltage associated to the MPP given the P-V curve, and V_{MPPT} presents the voltage where each MPPT operates according to its efficiency.

$$Power\ aptitude = \left(1 - \frac{MPP - MPPT}{MPP}\right) \times 100 \tag{5.1}$$

$$Voltage\ aptitude = \left(1 - \frac{V_{MPP} - V_{MPPT}}{V_{MPP}}\right) \times 100 \tag{5.2}$$

Table 5.1 shows the results based on Eq. 5.1 and 5.2. The precision is around 99% for the three algorithms, where the KF operates closer to the MPP, achieving 99.5%, since its operation is based on the P-V curve slope, making the prediction depending on the lightness or the steepness of the slope.

Algorithms	$P\&O$	Kf	PSO
Aptitude	98.8%	99.5%	99%

Table 5.1: Aptitude to achieve the MPP.

Oscillation around the MPP

The efficiency of each algorithm depends strongly on the amount of oscillation around the MPP in steady-state, since it represents an energy loss of the system. However, the amount of losses differs from one technique to another according to its operating principle. The oscillation of each MPPT can be analyzed as follows:

- Case of the $P\&O$ algorithm

  Figure 5.11 presents a zoom of Fig. 5.5 in the steady-state region, where the voltage

oscillation around the V_{MPP} $(129.5V)$ is permanent and periodic due to the fixed step of the perturbation imposed by the $P\&O$ algorithm $(4V)$. This situation leads to generate a power oscillation of about $\mp 14.5W$ from the average PV output power. However, This techniques presents a compromise between the amount of oscillation and the response time by the mean of the perturbation.

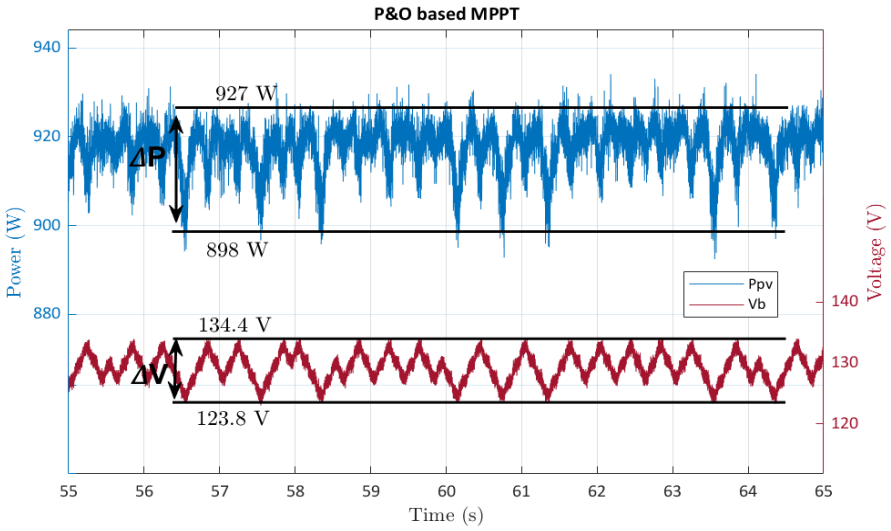

Figure 5.11: Oscillation around the MPP using PO technique

- Case of the KF algorithm

  Figure 5.12 presents a zoomed part of Fig. 5.6 in the steady-state region, where the oscillations around the V_{MPP} $(125.8V)$ are lower compared to the $P\&O$ technique, and not periodic since the KF has the ability to predict adaptatively the next voltage using the instantaneous power slope, whereas the $P\&O$ algorithm move to the next voltage with a fixed value. On the other hand, the KF technique reduces oscillations due to the power line and sensor noises by using their covariances at every iteration. Likewise, the oscillations around the MPP are lower compared to the $P\&O$, and about $\mp 11W$ from the mean output power.

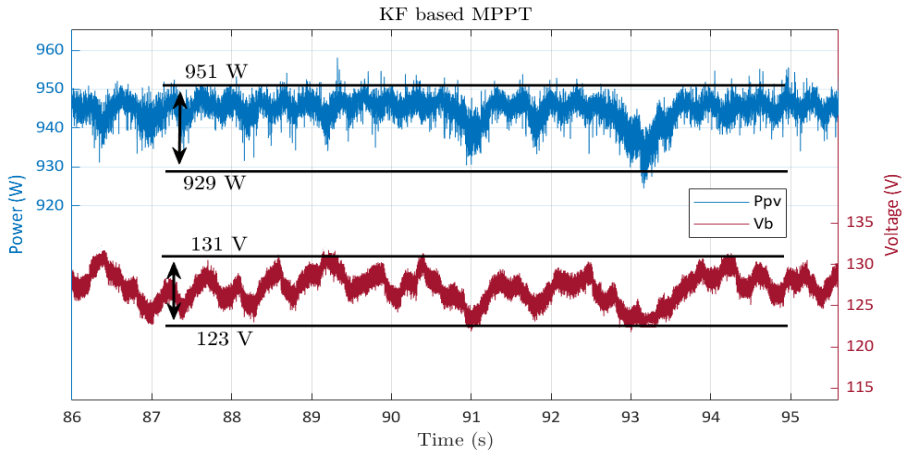

Figure 5.12: Oscillation around the MPP using KF technique

- Case of the PSO algorithm

  Figure 5.13 represents a zoomed part of Fig. 5.7 in steady-state, where the oscillations around the V_{MPP} are quite low compared to the $P\&O$ and the KF algorithms, and in a range of $(\mp 2V)$. Due to the fact that all duty cycles reach a better fitness value, where the direction of the velocity of these particles keeps unchanged and they then shift towards G_{best} in the same direction. As a result, the value of the duty cycle approaches a fixed constant, in which the operating point is maintained and the oscillation around the PPM decreases.

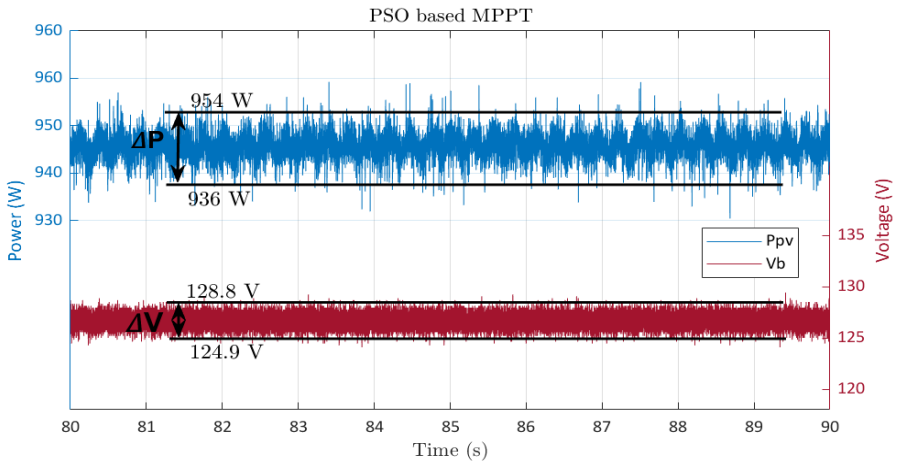

Figure 5.13: Oscillation around the MPP using PSO technique

Table 5.2 summarizes the amount of oscillation around the MPP and the V_{MPP} of the evaluated techniques.

MPPT	$P\&O$	KF	PSO
Delta P	1.6%	1.17%	0.96%
Delta V	4.13%	3.1%	1.54%

Table 5.2: Oscillation around the MPP.

Convergence speed

It is also called the response time and refers to the time taken from launching the MPPT technique ($40V$) until achieving the MPP. Based on the results obtained under normal operating conditions, the $P\&O$ algorithm achieves the MPP after $2.4s$, being the convergence speed affected by the perturbation factor, whereas the PSO algorithm took $2.8s$, where speed is affected directly by the social and cognitive components. Moreover, the initial oscillation presented by the PSO in Fig. 5.13, is due to the number of initial particles, which may also slow the response time by keeping the particles moving around the research space permanently. While the KF algorithm presents the higher convergence speed compared with the $P\&O$ and PSO algorithms, at around $2.3s$, since it moves to the next iteration adaptatively starting with a large step, then decreases this step when the MPP is closer to the V_{MPP} achieved by the algorithm. It is important to note that the execution cadence (the execution cycle) for the three MPPT is chosen to be $0.1s$. To avoid absolute value problems, the same test was repeated for different cadence values, in which the convergence speed was a multiple of the first one (0.1s). Table 5.3 summarizes the convergence speed of the three evaluated MPPTs.

MPPT	$P\&O$	KF	PSO
C. speed	$2.4s$	$2.3s$	$2.8s$

Table 5.3: Convergence speed of the MPPT evaluated.

Ability to deal with partial shadow

According to Fig. 5.8, 5.9 and 5.10, the $P\&O$ and KF techniques fail to operate around the global MPP, since they converge to the first optimum met, i.e. they confuse between the local optimum and global optimum. In fact, only the PSO was able to track the global MPP since it explores all over the research space with multiple particles in different directions, and compares their output power associated at every iteration in order to identify and track the global optimum.

Chapter 6

Conclusion and future work

6.1 Conclusion

This master thesis presents an experimental evaluation of one of the most unknown techniques in the tracking of the maximum power for photovoltaic systems, which is is the Kalman filter (KF) technique. The evaluation is based on experimental comparison with two of the most widely used algorithms, which are the Perturbation and Observation (P&O) and Particle Swarm Optimization (PSO). The contribution of this work was published in the International Journal of Renewable Energy and Research (IJRER) [17].

The experimental tests were curried out in the LSE with a grid connected PV system, using $Matlab/Simulink_{2011}$ and $dSpace\ real-time\ controller\ board$. The power topology is based on a boost converter followed by a voltage source inverter. The first controls the operating point of the PV string by setting its output voltage (input voltage of the boost converter). For this purpose, the MPPT algorithm gives the reference signal for the boost converter. The second controls the active power flow to the grid using voltage oriented control. This is done setting the DC-link voltage equal to 400V and controlling the current direct component in a reference frame synchronous with the grid voltage. The evaluation was based on two different configuration: under normal operating conditions and under partial shading.

One important conclusion from Chapter 3 is that the three evaluated MPPT algorithms differ in their operating principle, sensors required, complexity of implementation and initial parametrization, which play a key role in the tracking performances of each technique.

The experimental results assert that the KF algorithm exhibits a wide range of qualities superior to those of the P&O and PSO algorithms in terms of operating accuracy close to MPP, oscillation around MPP and convergence speed, which are summarized in Table 6.1. However, the KF shares the same drawback as P&O in partial shading, where they fail to distinguish between local and global optima, which leads to converge to the first optimum encountered. Unlike PSO, which was the only algorithm to handle partial shading, since its operation is based on exploring and exploiting the whole search space.

Algorithms	$P\&O$	KF	PSO
Aptitude	98.8%	99.5%	99%
Power oscillation	1.6%	1.17%	0.96%
Voltage oscillation	4.13%	3.1%	1.54%
Response time (s)	2.4	2.3	2.8
Ability in partial shading	No	No	Yes

Table 6.1: summary of the results obtained.

6.2 Future work

It would be interesting in future work to integrate the Kalman filter, which has great qualities under normal operating conditions, with particle swarm optimization to overcome the power loss due to shading, in order to develop a new powerful MPPT based on KF & PSO duality.

Bibliography

[1] M. Kumar, "Social, economic, and environmental impacts of renewable energy resources", *Wind Solar Hybrid Renewable Energy System*, 2020.

[2] A. Sambo, I. Zarma, P. Ugwuoke, I. Dioha, and Y. Ganda, "Implementation of standard solar PV projects in Nigeria", *Journal of Energy Technologies and Policy*, vol. 4, no. 9, pp. 22–28, 2014.

[3] M. N. Dehedkar and S. V. Murkute, "Optimization of PV system using distributed MPPT control", in *2018 International Conference on System Modeling & Advancement in Research Trends (SMART)*, IEEE, 2018, pp. 216–220.

[4] G. Masson and A. Detollenaere, "Snapshot of Global PV Markets 2020", The International Energy Agency- Photovoltaic Power Systems Programme, Tech. Rep., 2020.

[5] V. Smil, *Energy- A Beginner's Guide*. Oneworld Publications, 2012, ISBN: 978–1–85168–452–6.

[6] S. Wall, X.-C. Hong, L. Sha, and J.-R. Xie, "High-efficiency PV inverter with SiC technology", *IET Renewable Power Generation*, vol. 12, no. 2, pp. 149–156, 2017.

[7] N. Eswar, "Performance Study of Incremental Conductance and Modified Incremental Conductance MPPT Algorithms for Photovoltaic Applications", *International Journal of Science- Engineering and Technology Research (IJSETR)*, vol. 5, 2016.

[8] L. M. Fraas, *Low-Cost Solar Electric Power*. Springer International Publishing, 2014.

[9] A. Chandwani and A. Kothari, "Design, simulation and implementation of Maximum Power Point Tracking (MPPT) for solar based renewable systems", in *2016 International Conference on Electrical Power and Energy Systems (ICEPES)*, IEEE, 2016, pp. 539–544.

[10] V. K. Viswambaran, A. Ghani, and E. Zhou, "Modelling and simulation of maximum power point tracking algorithms & review of MPPT techniques for PV applications", in *2016 5th International Conference on Electronic Devices, Systems and Applications (ICEDSA)*, IEEE, 2016, pp. 1–4.

[11] C. Jaen, J. Pou, G. Capella, A. Arias, and M. Lamich, "On the use of sun trackers to improve maximum power point tracking controllers applied to photovoltaic systems", in *2009 Compatibility and Power Electronics*, IEEE, 2009, pp. 67–72.

[12] S. Motahhir, A. Aoune, A. El Ghzizal, S. Sebti, and A. Derouich, "Comparison between Kalman filter and incremental conductance algorithm for optimizing photovoltaic energy", *Renewables: Wind, Water, and Solar*, vol. 4, no. 1, pp. 1–10, 2017.

[13] B. O. Kang and J. H. Park, "Kalman filter MPPT method for a solar inverter", in *2011 IEEE Power and Energy Conference at Illinois*, IEEE, 2011, pp. 1–5.

[14] O. B. Belghith, L. Sbita, and F. Bettaher, "Maximum power point tracking by the technique of the extended Kalman filter", in *2017 International Conference on Green Energy Conversion Systems (GECS)*, IEEE, 2017, pp. 1–5.

[15] R. ROY, "Application of kalman filter in maximum power point tracking of solar photovoltaic cell", *International Journal of Advance Engineering and Research Development*, vol. 5, 2018.

[16] M. H. Rashid *et al.*, *Power electronics handbook: devices, circuits, and applications/edited by Muhammad H. Rashid.* 2011.

[17] M. Chellal, T. Guimarães, and V. Leite, "Experimental Evaluation of MPPT algorithms: A Comparative Study", *to be published in the International Journal of Renewable Energy Research*, 2021.

[18] A. E. G. Alonso, "Maximum Power Point Tracking Algorithms for Solar Photovoltaic Systems", *Universidad Politécnica de Madrid, Madrid*, 2017.

[19] M. G. Hudedmani, V. Soppimath, and C. Jambotkar, "A Study of Materials for Solar PV Technology and Challenges", *European Journal of Applied Engineering and Scientific Research*, vol. 5, pp. 1–13, 2017.

[20] M. M. A. Bagher M. Abadi Vahid, "Types of Solar Cells and Application", *American Journal of Optics and Photonics*, Aug. 2015.

[21] HomeAdvisor. (Last access 27/03/2021). Price of Solar Panels, [Online]. Available: `https://www.homeadvisor.com/cost/heating-and-cooling/solar-panel-prices`.

[22] M. Svarc, "Most Efficient Solar Panels 2021", Clean Energy Reviews, 2021 (Last access 27/03/2021).

[23] M. G. Villalva, J. R. Gazoli, and E. Ruppert Filho, "Comprehensive approach to modeling and simulation of photovoltaic arrays", *IEEE Transactions on power electronics*, vol. 24, no. 5, pp. 1198–1208, 2009.

[24] M. Taherbaneh, G. Farahani, and K. Rahmani, "Evaluation the accuracy of one-diode and two-diode models for a solar panel based open-air climate measurements", *Solar Cells-Silicon Wafer-Based Technologies*, vol. 4, pp. 201–228, 2011.

[25] J. Gow and C. Manning, "Development of a photovoltaic array model for use in power-electronics simulation studies", *IEE Proceedings-Electric Power Applications*, vol. 146, no. 2, pp. 193–200, 1999.

[26] K. Nishioka, N. Sakitani, Y. Uraoka, and T. Fuyuki, "Analysis of multicrystalline silicon solar cells by modified 3-diode equivalent circuit model taking leakage current through periphery into consideration", *Solar energy materials and solar cells*, vol. 91, no. 13, pp. 1222–1227, 2007.

[27] N. Pandiarajan, "Mathematical modeling of photovoltaic module with Simulink", *International Conference on Electrical Energy Systems*, Feb. 2011.

[28] P. Singh and N. M. Ravindra, "Analysis of series and shunt resistance in silicon solar cells using single and double exponential models", *Emerging Materials Research*, vol. 1, no. 1, pp. 33–38, 2012.

[29] F. M. González-Longatt *et al.*, "Model of photovoltaic module in Matlab", *Ii Cibelec*, vol. 2005, pp. 1–5, 2005.

[30] O. M. Akeyo, *Analysis and simulation of photovoltaic systems incorporating battery energy storage*, 2017.

[31] J. J. B. Alsayid S. Alsadi and M. Dradi, "Partial Shading of PV System Simulation with Experimental Results", vol. 4, pp. 429–435, 2013.

[32] F. Belhachat and C. Larbes, "Modeling, analysis and comparison of solar photovoltaic array configurations under partial shading conditions", *Elsevier*, no. 120, pp. 399–418, 2015.

[33] M. Abdulkadir, A. Bukar, and B. Modu, "MPPT-based control algorithm for PV system using iteration-PSO under irregular shadow conditions", *Arid Zone Journal of Engineering, Technology and Environment*, vol. 13, no. 1, pp. 97–110, 2017.

[34] K. Yadav, B. Kumar, and D. Swaroop, "Mitigation of mismatch power losses of PV array under partial shading condition using novel odd even configuration", *Energy Reports*, vol. 6, pp. 427–437, 2020.

[35] S. L. A. Dolara G. Cristian Lazaroiu and G. Manzolini, *Experimental investigation of partial shading scenarios on PV (photovoltaic) modules*. Energy, Jun. 2013.

[36] A. M. Ajmal, T. S. Babu, V. K. Ramachandaramurthy, D. Yousri, and J. B. Ekanayake, "Static and dynamic reconfiguration approaches for mitigation of partial shading influence in photovoltaic arrays", *Sustainable Energy Technologies and Assessments*, vol. 40, p. 100 738, 2020.

[37] D. Sera, "Real-time Modelling, Diagnostics and Optimised MPPT for Residential PV Systems", Denmark: Institute of Energy Technology, 2009.

[38] S. Bimenyimana *et al.*, "Optimization comparison of stand-alone and grid-tied solar PV systems in Rwanda", *Open Access Library Journal*, vol. 5, no. 05, p. 1, 2018.

[39] S. P. Word, *Oversize MPPT controllers in off-grid systems for more ROI*, `https://www.solarpowerworldonline.com/2018/03/oversize-mppt-controllers-off-grid-systems-roi`, 2018 (Visited on February. 02,2021).

[40] P. Bhatnagar and R. Nema, "Maximum power point tracking control techniques: State-of-the-art in photovoltaic applications", *Renewable and Sustainable Energy Reviews*, vol. 23, pp. 224–241, 2013.

[41] K. S. Sumathi and P. Surekha, *Solar PV and Wind Energy Conversion Systems*, 1st. Switzerland: Green Energy and Technology, 2015, ISBN: 978-3-319-14941-7.

[42] D. Sera, T. Kerekes, R. Teodorescu, and F. Blaabjerg, "Improved MPPT algorithms for rapidly changing environmental conditions", in *2006 12th International Power Electronics and Motion Control Conference*, IEEE, 2006, pp. 1614–1619.

[43] M. Farhat, O. Barambones, and L. Sbita, "A real-time implementation of MPPT-based on P&O method", in *2016 5th international conference on electronic devices, systems and applications (ICEDSA)*, IEEE, 2016, pp. 1–5.

[44] A. Al-Diab and C. Sourkounis, "Variable step size P&O MPPT algorithm for PV systems", in *2010 12th International Conference on Optimization of Electrical and Electronic Equipment*, IEEE, 2010, pp. 1097–1102.

[45] N. Femia, G. Petrone, G. Spagnuolo, and M. Vitelli, "Optimizing sampling rate of P&O MPPT technique", in *2004 IEEE 35th Annual Power Electronics Specialists Conference (IEEE Cat. No. 04CH37551)*, IEEE, vol. 3, 2004, pp. 1945–1949.

[46] J. Kennedy and R. Eberhart, "Particle swarm optimization", in *Proceedings of ICNN'95-international conference on neural networks*, IEEE, vol. 4, 1995, pp. 1942–1948.

[47] K. E. Parsopoulos and M. N. Vrahatis, *Particle swarm optimization and intelligence: advances and applications: advances and applications*. IGI global, 2010.

[48] S. Hadji, "Optimisation de la conversion énergétique pour les systèmes à énergie Photovoltaıque", PhD thesis, 2018.

[49] K. Ishaque, Z. Salam, M. Amjad, and S. Mekhilef, "An improved particle swarm optimization (PSO)–based MPPT for PV with reduced steady-state oscillation", *IEEE transactions on Power Electronics*, vol. 27, no. 8, pp. 3627–3638, 2012.

[50] T. F. Guimarães and V. Leite, "Analyses of MPPT Algorithms in Real Test Conditions", in *2020 9th International Conference on Renewable Energy Research and Application (ICRERA)*, IEEE, 2020, pp. 164–169.

[51] V. Ramchandani, K. Pamarthi, N. Varma, and S. R. Chowdhury, "Implementation of Maximum Power Point Tracking Using Kalman Filter for Solar Photovoltaic Array on FPGA", *International Journal of Smart Grid and Clean Energy*, vol. 2, no. 2, pp. 152–158, 2013.

[52] C. K. Chui and C. Guanrong, *Kalman Filtering with Real-Time Applications*. Springer, Berlin, Heidelberg, 1987, vol. 17, pp. 1–19.

[53] S. Haykin, *Kalman filtering and neural networks*. John Wiley & Sons, 2004, vol. 47.

[54] B. O. Kang, "Maximum power point tracking using Kalman filter for photovoltaic system", PhD thesis, Virginia Tech, 2010.

[55] P. Kim, *Kalman Filter for Beginners: with MATLAB Examples*. CreateSpace, 2011, vol. 6.

[56] V. Leite, Ferreira, and J. Batista, "Bidirectional vehicle-to-grid interface under a microgrid project", in *2014 IEEE 15th Workshop on Control and Modeling for Power Electronics (COMPEL)*, IEEE, 2014, pp. 1–7.

[57] M. M. Breve and V. Leite, "Control of a Bidirectional Single-Phase Grid Interface for Electric Vehicles", in *Ibero-American Congress of Smart Cities*, Springer, 2019, pp. 285–299.

Appendix A

Measurement noise covariance calculation

The covariance formula can be written as:

$$\sigma_x \times \sigma_y = \frac{\sum_{n=1}^{N}(\overline{x} - x_i) \times (\overline{y} - y_i)}{N} \tag{A.1}$$

Since the system is a one-dimensional system, the covariance becomes variance following Eq. A.2.

$$\sigma_x^2 = \frac{\sum_{n=1}^{N}(\overline{x} - x_i)^2}{N} \tag{A.2}$$

In order to estimate the measurement covariance noise, which refers to the uncertainties of the voltage sensor, the PV output voltage must be measured. Right after, a portion of data from the measured voltage in steady-state has to be exported to excel software. At the end, using Eq. A.3, the measured covariance noise. By fixing this last, the process error covariance can be tuned and concluded by trials.

$$\sigma_{V_{meas}}^2 = \frac{\sum_{n=1}^{N}(\overline{V_{meas}} - V_{meas,i})^2}{N} \tag{A.3}$$

Appendix B

Published article

Title: Experimental Evaluation of MPPT Algorithms:A Comparative Study.

Published in: International Journal of Renewable Energy Research (IJRER).

Published on: 02 April 2021.

Journal Location: Turkey.

Experimental Evaluation of MPPT Algorithms: A Comparative Study

Majd Chellal*‡, Thiago Fialho Guimarães**, Vicente Leite***

*Superior School of Applied Sciences, BP 165 RP Bel horizon 13000 Tlemcen, Algeria

**Technological Federal University of Paraná, Curitiba-PR, 80230-901, Brazil

***Research Centre in Digitalization and Intelligent Robotics (CeDRI), Polytechnic Institute of Bragança, Campus de Santa Apolónia - 5300-253 Bragança, Portugal

(majdchellal7@gmail.com, thiagofialho.vg@gmail.com, avtl@ipb.pt)

‡Corresponding Author; First Author, Road Aquilino Ribeiro Nº 2, 5300-087 Bragança, Portugal,

Tel: +351 934 477 681, majdchellal7@gmail.com

Received: 16.02.2021 Accepted:11.03.2021

Abstract- Photovoltaic (PV) energy is among the most used renewable sources. Grid-connected PV systems should yield as much energy as possible. However, external influencers such as irradiance and temperature impose a non-linear characteristic of the PV system, which hinder its operation at the maximum power point. Additionally, other factors, such as shading or internal degradation, can change this characteristic by making local maximums appear, which makes it difficult to extract the maximum available power. There are several techniques for maximum power point tracking (MPPT) and very diverse algorithms for this purpose. There are also some published works with comparative studies. However, in most of these works, the comparison is based on a literature review or on simulation. An experimental evaluation of MPPT techniques, from the simplest to the most complex, remains relevant. Thus, this paper presents an experimental analysis of five MPPT algorithms: two of the simplest and widely used (Perturb & Observe and Incremental Conductance) and three of the most complex (Fuzzy Logic Controller, Kalman Filter and Particle Swarm Optimization). The experimental tests were carried out under real test conditions, using Simulink and the dSPACE 1103 real-time controller board. The results show that the five MPPT algorithms are able to track the MPP with a difference of less than 2% in their efficiency under normal operating conditions. This difference increases under shadow effect. The PSO algorithm was the only one able to find the global MPP under the effect of partial shading.

Keywords MPPT algorithms; Perturb and Observe; Incremental Conductance; Fuzzy Logic Control; Kalman filter; Particle Swarm Optimization.

1. Introduction

Since the past decade, photovoltaic (PV) energy is among the most preferred source over all the other renewable sources, due to its wide range of qualities such as abundance in nature, low maintenance and high power density [1, 2]. However, the efficiency of PV systems is greatly affected by the efficiency of the inverter, the PV modules and the maximum power point tracking (MPPT) algorithms. PV inverters available on the market have achieved a maximum efficiency of 98% [3]. The increase of PV modules efficiency is under way and has been intensely investigated but it depends on complex manufacturing processes. Instead, improving the efficiency of the MPPT with various control techniques may be an alternative [4]. The main goal of these algorithms is to achieve the maximum power point (MPP) located along the nonlinear P-V characteristic, which depends on the temperature, solar irradiance and shadow situations [5]. Fig. 1 presents a generic P-V curve under normal test conditions containing a unique MPP, and under partial shading conditions, which contains a local MPP (LMPP) and a global MPP (GMPP)[5, 6].

There are about 10 main MPPT techniques [7, 8], and a few dozen variants [9] published in literature. Some of the most recent works [10-12] deal with the integration of conventional

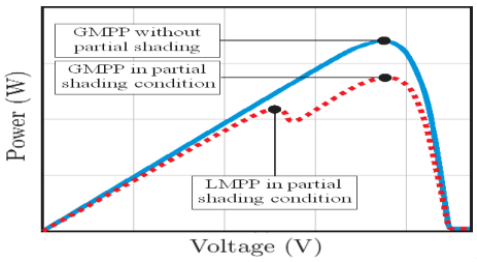

Fig. 1. Generic P -V curves.

and advanced MPPT techniques, since conventional techniques are very complex to implement [13]. In [5], research lacunae and noteworthy remarks are discussed on recently published MPPT algorithms. Most research work focuses on simulation for the purposes of cost and versatility analysis [14, 6], which leads to a lack of information regarding other characteristics. Furthermore, the MPPT based on the Kalman filter has not been sufficiently investigated since only a few simulation studies are known [15–17].

This paper presents an experimental evaluation between different MPPT techniques such as Perturb and Observe (P&O), Incremental Conductance (IC), Fuzzy Logic Controller (FLC), Kalman Filter (KF) and Particle Swarm Optimization (PSO). It compares the performance of these algorithms in terms of oscillation at the MPP, precision of the MPP voltage and shadow effect. The paper brings an experimental perspective, which complement many studies reporting analytical or simulation studies. Furthermore, this paper presents further developments to the previous work [18] with the analysis of the KF algorithm about which there is still lack of information regarding the MPPT capabilities.

The practical implementation of the MPPT algorithms was carried out using a conventional power topology based on a step-up converter followed by a single-phase voltage source inverter under Voltage Oriented Control (VOC) [18]. Both, MPPT and VOC algorithms were implemented in Simulink and tested using the dSPACE 1103 real-time controller board and ControlDesk interface.

2. MPPT Control Algorithms

References [2, 19] present a wide comprehensive review of published algorithms for MPPT, but it does not include the Kalman filter strategy. This section summarizes the MPPT algorithms evaluated in this paper by extending the previous description made in [18] to the Kalman filter technique.

2.1. Perturb and Observe

Perturb and Observe (P&O) technique is the most used and cited in literature due to its simplicity of implementation [19]. The algorithm measures the PV voltage and current to calculate the PV output power. Then, it introduces a perturbation on the voltage reference and observes the effect on the output power. If it increases, the perturbation of the next iteration will continue in the same direction. Otherwise, the direction of the perturbation will be reversed [20-22]. Fig. 2 shows the flowchart of the P&O algorithm.

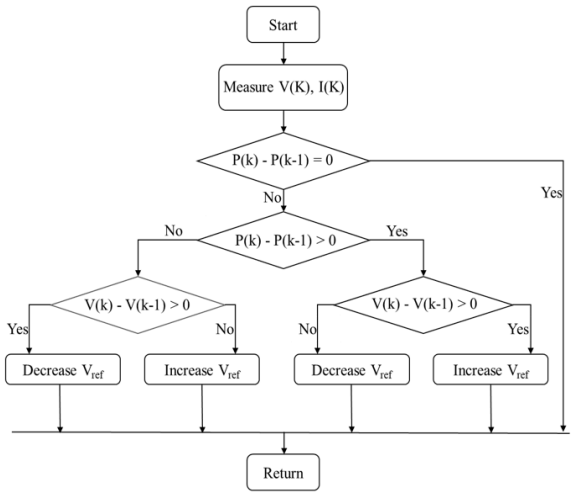

Fig. 2. Flowchart of Perturb and Observe algorithm.

2.2. *Incremental Conductance*

Considering the convex aspect of the P-V characteristic, the incremental conductance (IC) algorithm is based on the fact that the slope of the P-V curve is equal to zero $\left(\frac{\Delta P}{\Delta V} = 0\right)$ at the MPP [19]. Eq. (1) presents the operating principle of the IC technique:

$$\begin{cases} \dfrac{\Delta I}{\Delta V} = -\dfrac{I}{V} \; if \; P = MPP \\ \dfrac{\Delta I}{\Delta V} > -\dfrac{I}{V} \; if \; P < MPP \\ \dfrac{\Delta I}{\Delta V} < -\dfrac{I}{V} \; if \; P > MPP \end{cases} \tag{1}$$

The MPP is achieved by comparing the incremental conductance $\left(\frac{\Delta P}{\Delta V}\right)$ with the instantaneous conductance $\left(\frac{I}{V}\right)$. Fig. 3 presents the IC technique flowchart, where the algorithm increases or decreases the reference voltage until the condition $\frac{\Delta I}{\Delta V} = -\frac{I}{V}$ is atained [15].

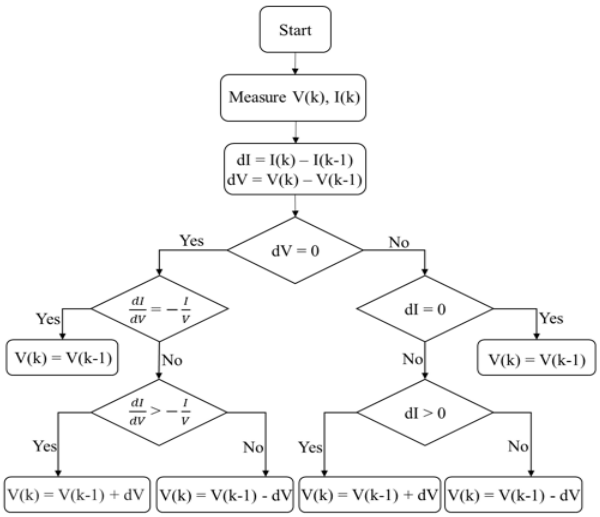

Fig. 3. Flowchart of Incrimental Inductance algorithm.

2.3. Particle Swarm Optimization

The Particle Swarm Optimization (PSO) algorithm begins with an initial swarm of random particles throughout the research space, where the generation update is completed until the optimal solution is found. Each individual has his own fitness value, which is measured frequently in order to select the optimal individual to continue with the next generation. Each individual has only two values where the first is the personal best $(P_{best,i})$ and the second is the global best (G_{best}). The personal best is for each particle while the global best is a unique one for all the particles of the swarm [19, 23]. In short, each particle tries to improve its current location and velocity based on two criteria: the path between its present location and its personal best location, and the distance between its present location and the global best, relative to all the particles. For the MPPT purpose, the operation starts by searching the nearest point to the MPP using the PSO optimization, where the duty cycle of the DC-DC converter represents the position (Particle location) and the output power refers to the fitness function (maximum character function). The PSO flowchart is shown in Fig. 4. The following equations are used to adjust the new position at each iteration, Eq. (3), via the speed equation given by Eq. (2) [24].

$$v_i(k+1) = w\, v_i(k) + C_1 R_1\big(P_{best,i} - D_i(k)\big) + C_2 R_2(G_{best} - D_i(k)) \quad (2)$$

$$D_i(k+1) = D_i(k) + v_i(k+1) \quad (3)$$

D_i and v_i are the duty cycle and the velocity of the particle i, respectively, and C_1 and C_2 are the acceleration constants. w refers to the weight of inertia and R_1 and R_2 are random values between 0 and 1. $P_{best,i}$ is the location with the best fitness of all the visited locations of the particle i, and G_{best} is the best position found over all the particles. In this work, the number of initial particles is chosen to be 4, C_1 and C_2 are 1.2 and 2 respectively, and w equal to 0.4.

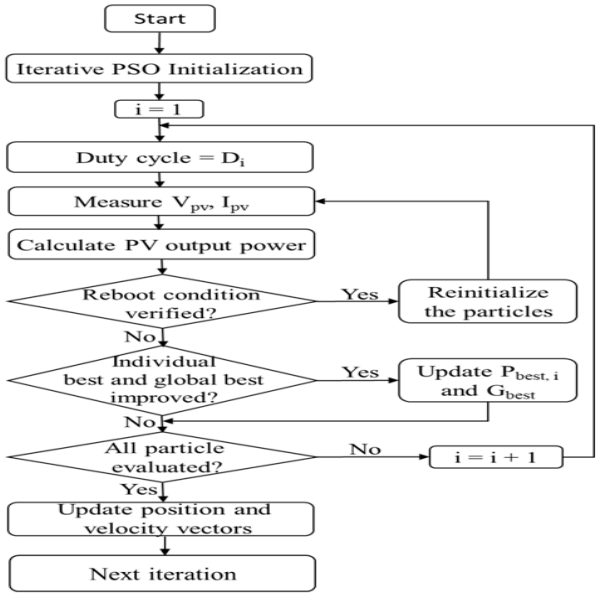

Fig. 4. Flowchart of Particle Swarm Optimization algorithm.

2.4. Kalman Filter

The Kalman filter (KF) technique was applied in [16] for MPPT purposes and compared with the P&O algorithm. Recently, other works [15, 17] have done similar studies. Reference [15] presents a comparison between KF and the IC method and in [17] the comparison is with the PSO algorithm. These works present their analysis using simulation results. This work extends the previous experimental research [18] (with P&O, IC and PSO) to the KF and makes the analyses based on experimental results.

The KF is a recursive identification method used for systems described by a state-space representation. However, in this case, it takes into consideration the system (r_s) and measurement (r_m) noises. The first represents the imperfections of the modeling process and controllers. The second represents the imperfections of measurements. This stochastic state-space representation is described by the following equations [25]:

$$x(k+1) = Ax(k) + Bu(k) + r_s(k) \quad (4.a)$$

$$y(k) = Cx(k) + r_m(k) \quad (4.b)$$

The first is the state equation and the second is the output equation, where u and y represent, respectively, the input and output of the system. The state vector is composed by only one state variable: the PV string output voltage reference. This is the reference for the input voltage of the step-up converter as shown in Fig. 5. In a general case, if the matrices A, B and C are constant, each state variable of the state vector x do not depend on other state variables of the same state vector. In that case, the state-space representation (4) is linear and the Kalman filter can be applied. The state-space equations (4) can be applied to the MPPT as demonstrated in [15–17]. Both, r_s and r_m, are considered Gaussian and independent sequences. The system output, $y(k)$, is the PV string output voltage and the system input, $u(k)$, is the slope of the P-V curve, $\frac{\Delta P}{\Delta V}(k)$. In this case $A = B = 1$ and B is a scaling factor M as described in [15–17].

The KF is a recursive state estimator method and, in each iteration, it has two steps: prediction and estimation. In the first, it predicts the state variable $V(k+1|k)$ and the process covariance value $P(k+1|k)$, considering the information available at instant k [17]. The Kalman gain $K(k+1)$ is then calculated using these predictions. This step requires the process noise covariance value, Q, and the measurement error value (sensor noise covariance), R. These values represent the lack of confidence, respectively, in the predicted state and in the measures. Usually these values are obtained by a trial and error process and require some experience.

In the second step, the algorithm estimates the state variable and the process covariance considering the previous information already available at the instant $k+1$, respectively, $V(k+1|k+1)$ and P $(k+1|k+1)$. The KF algorithm is described in Fig. 6. The two first equations (prediction step) represent the voltage and the process

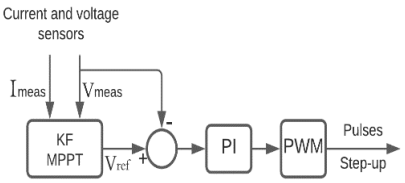

Fig. 5. Step-up converter control using KF for MPPT and a PI controller.

covariance predicted by the algorithm, respectively, $V_p(k)$ and $P_p(k)$. The last three equations represent the estimation step. The computation of the Kalman gain $K(k)$ requires the measurement error covariance value R and the predicted process covariance value, $P_p(k)$, which in turn requires the process noise covariance value Q. After that, the state variable (step-up input voltage reference) is updated by the Kalman gain times the error between the measured voltage, $V(k)$, given by voltage sensor in Eq. (4b), and the predicted voltage $V_p(k)$. Finally, the process covariance value is updated at the same iteration, which tends to become closer and closer to zero [16, 17]. The required parametrization used in this work is summarized in Table 2. In this work, the scale factor is chosen to be 1, Q is equal to 0.25, and R equal to 0.31.

2.5. Fuzzy Logic Control

A fuzzy logic controller has three stages, fuzzification, inference mechanism and defuzzification as shown in Fig. 7 [26]. The fuzzification passes the real variables to fuzzy variables. The proposed fuzzy controller has two input variables: the voltage variation (ΔV) and the power variation (ΔP) [26]. In an instant of sampling, these variables are expressed as:

$$\Delta V(k) = V(k) - V(k-1) \quad (5)$$

$$\Delta P(k) = \Delta V(k) \times \Delta I(k) \quad (6)$$

The input signals ΔV and ΔP are converted to linguistic variables such as PB (big positive), PM (positive medium), PS (positive small), Z0 (zero), NS (small negative), NM (negative medium), NB (large negative) using the association functions. Fig. 8 shows the association functions used to input and output variables [27].

Fuzzy inference uses Mamdani's method and defuzzification is based on the centroid method to calculate the ΔV_{ref} output. Fig. 8 shows the rule base used to find the output and Eq. (7) gives the reference voltage for the PI controller (V_{ref}) [18].

$$V_{ref} = V \times \Delta V_{ref} \quad (7)$$

On the other hand, in the defuzzification, the fuzzy logic controller output is converted to a controller variable, which is used by the PI controller as the voltage reference (V_{ref}). Fuzzy logic controllers are able to work with inaccurate inputs and, therefore, they do not need a precise linear mathematical model, with a higher implementation cost [27].

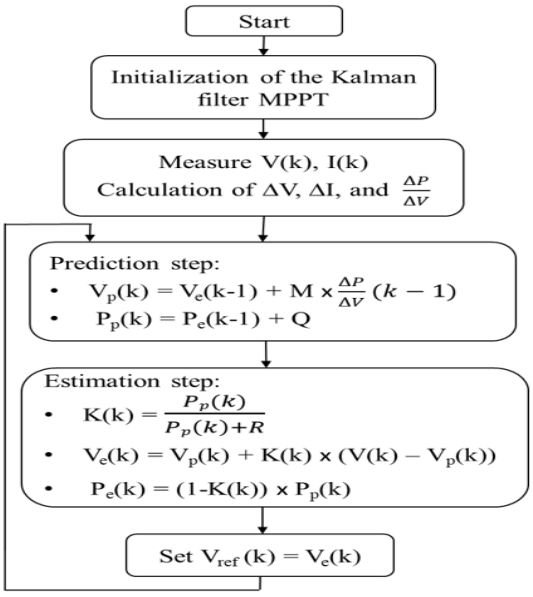

Fig. 6. Flowchart of Kalman Filter algorithm.

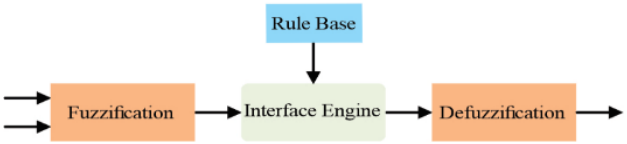

Fig. 7. Flowchart of Fuzzy Logic Controller algorithm.

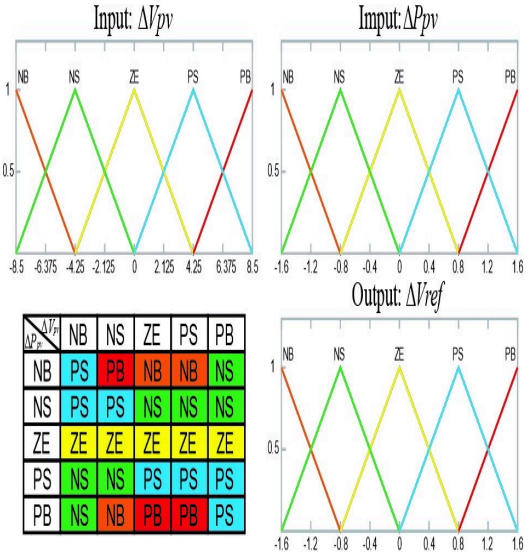

Fig. 8. Membership functions [18].

3. Power Topology, Control Strategy and Experimental Set-Up

Fig. 9(a) presents the power topology used in this work. It was implemented using the intelligent power module (IPM) PM75RLA120 from Powerex. This IPM is a three-phase IGBT inverter plus a brake IGBT. The latter is always kept OFF and the three-phase inverter is then configured in order

to obtain the desired power topology [28, 29]. Thus, the first leg (U) implements a boost converter by keeping the upper IGBT always OFF. The other two legs (V, W) implement a single-phase voltage source inverter (VSI). Fig. 9(b) shows the experimental set-up. It consists of the power structure, described in the previous paragraph, with an LC output filter and an isolation transformer used for a protection purpose. The measurement module is a signal conditioning interface for data acquisition and signal filtering. The dSPACE 1103 real-time controller board controls the boost converter and the single-phase VSI. The control and user interface are implemented using *Simulink* with *Real-Time Interface* and *ControlDesk*.

The control strategy implements independent control of the boost converter and the VSI. The first controls power extracted from the PV string by setting its operating voltage. The MPPT algorithms described in the previous section generate the reference voltage. Then, the PI controller is responsible for maintaining the output voltage of the PV string equal to the reference voltage given by the MPPT algorithm. Thus, it generates the control voltage for the PWM, as shown in Fig. 5. The second controls the power flow from the PV string to the grid by keeping the DC-link voltage constant at 400 V. For this purpose, the single-phase VSI is controlled using the voltage oriented control (VOC) strategy as in [28, 29]. The implemented VOC of the VSI is shown in Fig. 9(c). The grid current is converted to the fixed orthogonal reference frame $\alpha\beta$. For this purpose, a quadrature component is obtained by applying a 90º phase shift. This is carried out by a delay of a quarter of the grid period (0.25T) which generates the virtual orthogonal component, i_β. The resulting $\alpha\beta$ components are orthogonal sinusoidal currents. PI controllers can be used to control sinusoidal currents but there are two well-known drawbacks: they present steady-state errors with sinusoidal reference and are not able to reject disturbances. This is due to the poor performance of the integrative action when the reference is a periodic signal. To overcome this difficulty, the grid current $\alpha\beta$ components are converted to a dq reference frame synchronous with the grid voltage. In this new reference frame, the orthogonal components of the grid current are DC quantities and consequently, PI controllers can be used. Therefore, they are able to cancel the steady-state error, at the fundamental frequency of the grid, and improve its dynamic response [28, 29].

The-dq reference frame rotates with the same angular speed of the grid voltage and current, and the d axis is permanently aligned with the grid voltage space-phasor. In this way, the grid voltage quadrature component, V_{gq}, is zero and, therefore, the active and reactive powers are controlled independently by controlling, respectively, the d and q current components. The first is controlled by keeping the DC-link voltage constant, as described above, and the second is directly defined, making reactive power compensation possible. In order to obtain the grid voltage angle, θ, for reference frame transformation and synchronization, a Phase Locked Loop (PLL) block was implemented as in [28].

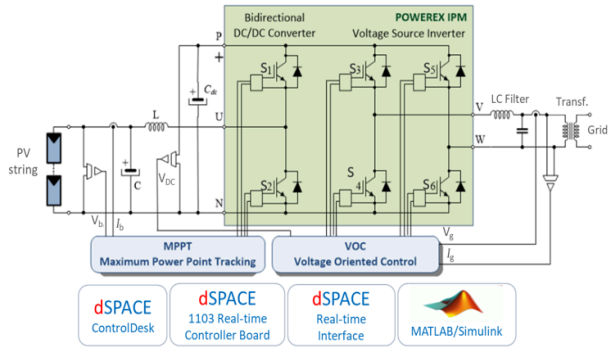

(a)

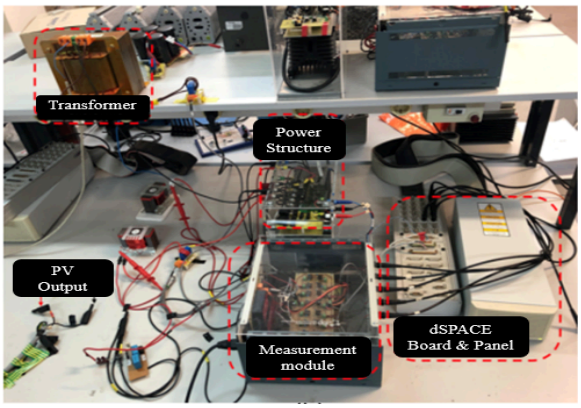

(b)

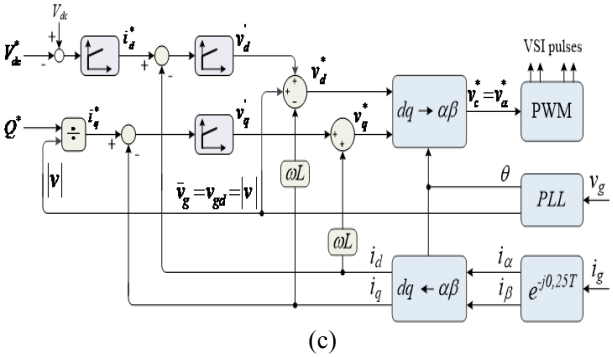

(c)

Fig. 9. Power structure (a), experimental set-up (b) and VSI control using VOC (c).

Fig. 10 shows the two PV strings used in this work. String A consists of 5 Fluitecnik FTS220P PV modules and string B consists of 3 REC 275PE PV modules. The technical characteristics of the PV modules are shown in Table 1.

Table 1. Characteristics of the PV modules.

String	$P_{max}(W)$	$I_{SC}(A)$	$V_{OC}(V)$	$I_{MPP}(A)$	$V_{MPP}(V)$
A	220	8.30	36.76	7.51	29.38
B	275	9.25	38.70	8.74	31.50

Fig. 10. PV string models [18].

4. Experimental Results

For the experimental tests, the two PV strings described above were used. Under normal operating conditions, all the algorithms were evaluated using PV string A, which has higher power available. The tests were carried on clean days where the irradiation and temperature are almost constant during the time of the test. This PV string is installed on the roof of the laboratory and there is wiring which allows making various configurations (series and parallel) of these modules inside the laboratory. However, for now, it is not very easy nor safe to access the roof. Therefore, due to the difficulty of access for shadow emulation, a second string (B) was placed in front of the laboratory for the tests with shading. Thus, the tests under shading conditions were carried out using PV string B for all algorithms. Immediately before each test, the P-V curve was traced to obtain the MPP.

The PV modules of string B are made up of strings of 20 cells in series with bypass diodes. Thus, to cause a local maximum in the P-V curve, it is enough to shade at least one cell of each string. For this, a semitransparent film was used, as illustrated in Fig. 10.

Each algorithm was tested separately. The MPP voltage, given by each one, was used as a reference voltage for the step-up converter input. The power available on the DC-link was injected into the grid by controlling the single-phase VSI as described in the previous section.

4.1. Tests under normal operating conditions

Fig. 11 shows the experimental results obtained with the MPPT algorithms and string A. At the beginning of the tests, 65 % of the P-V curve is traced in order to identify the MPP. Thus, the control algorithm linearly increases string's output voltage from 40 V to 150 V, tracing the P-V curve and, therefore, passing through the MPP. Then, the algorithms start with an initial reference voltage of 40 V as shown in Fig. 11(a) to (d). The exception is the PSO algorithm. In this case, the duty cycle increases from 0.4 to 0.9 leading to a linear reduction in the output voltage of the PV string, making it pass through the MPP, as shown in Fig. 11(e).

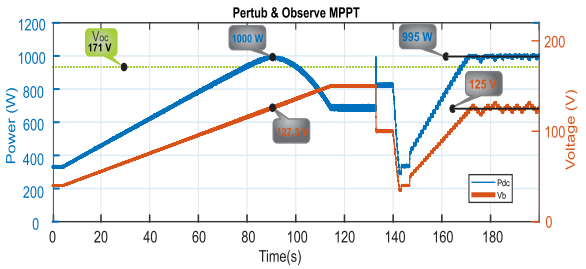

(a) Using P&O [18]

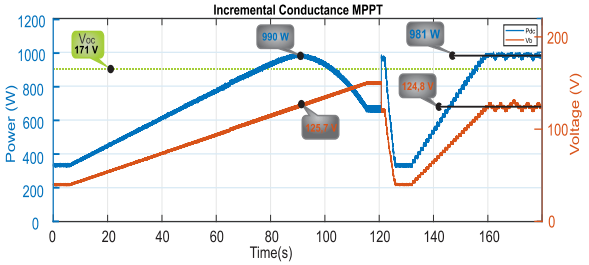

(b) Using IC [18]

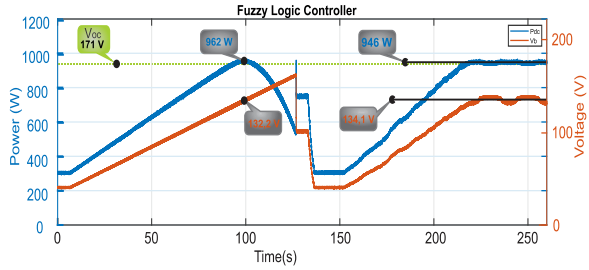

(c) Using FLC [18]

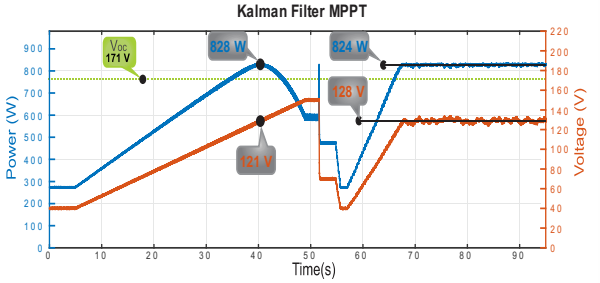

(d) Using KF

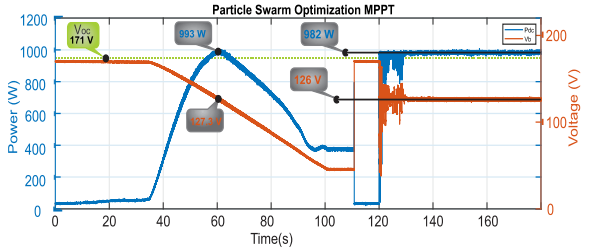

(e) Using PSO [18]

Fig. 11. MPPT algorithms evaluation tests under normal operating conditions.

4.2. Tests under Partial Shading

Fig. 12 shows the experimental results obtained with string B and the shading procedure described previously. The tests were performed as described in the previous section. First, the MPP is identified by tracing the P-V curve and then the algorithms are launched to track the MPP by starting at 40 V.

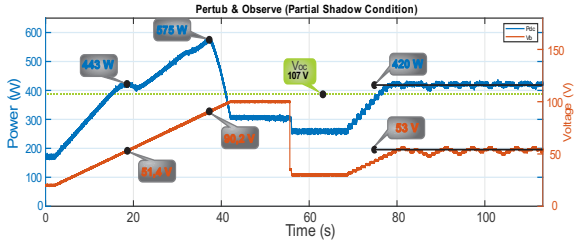

(a) Using P&O [18]

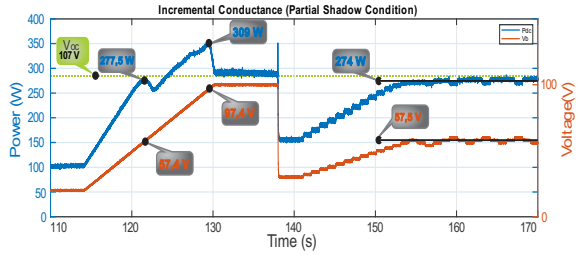

(b) Using IC [18]

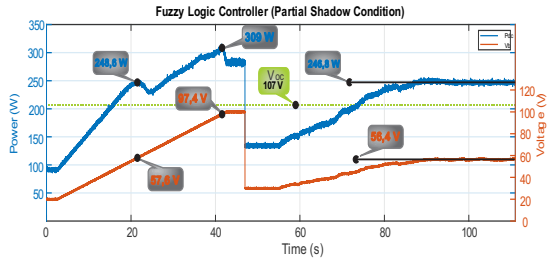

(c) Using FLC [18]

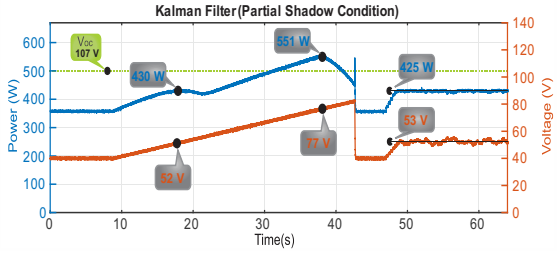

(d) Using KF

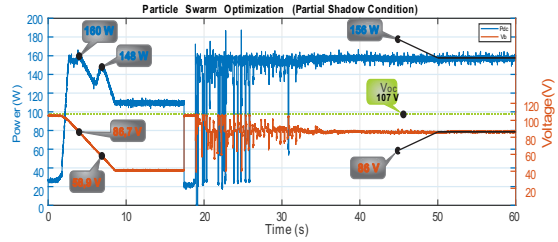

(e) Using PSO [18]

Fig. 12. MPPT algorithms evaluation tests under shading conditions.

5. Discussion

This section discusses the results presented in the previous section. According to the tests carried out, it is possible to compare the performance of each MPPT algorithm in terms of precision in reaching the MPP, oscillation around the MPP, and ability to find the global MPP in shadow situation.

5.1 Oscillation at the MPP

The oscillation around the MPP refers to the difference between the output power maximum and minimum values divided by the power at the MPP previously known, which affects the system efficiency.

Fig. 13 presents a more detailed graphical analysis of the operation of the algorithms after they have already reached the MPP. It shows, graphically, the oscillation in the operating values of power and voltage. The results of this analysis are summarized in Table 2, which presents the power and voltage oscillations of the evaluated MPPT algorithms. The results show that the oscillation is less than 2% with the best results obtained with the PSO and KF algorithms, respectively 0.95% and 1.12%.

It should be noted that MPPT algorithms such as P&O and IC were tested with fixed step increments or decrements in the reference voltage. The size of these steps is a tradeoff between the oscillation magnitude around the MPP and the response time to achieve the MPP. For the purpose of this study, and for the comparison of only conceptual versions, modified implementations as in [12] were not considered.

Table 2. Power and voltage oscillation around the MPP.

Oscilla.	***P&O***	***IC***	***PSO***	***FLC***	***KF***
ΔP	1.82%	1.77%	0.95%	1.60%	1.12%
ΔV	4.85%	4.79%	1.61%	3.70%	2.9%

5.2 Ability to achieve the MPP

The efficiency of each algorithm can be evaluated through the difference between the operating voltage imposed by the MPPT algorithm and the MPP voltage previously known (precision). Table 3 presents the ability to achieve the MPP for the evaluated algorithms using Eq. (8), where V_{MPP} is the MPP voltage given by the P-V curve, and V_{MPPT} is the voltage where each MPPT technique operates. The V_{MPPT} value used in Eq. (8) corresponds to the average value of the operating voltage after steady-state has been reached.

$$Precision = 100 \times \left(1 - \frac{(V_{MPP} - V_{MPPT})}{V_{MPP}}\right) \quad (8)$$

According to the results obtained, efficiency is around 99%, where the best results are obtained with KF and IC algorithms with 99.4% and 99.3% efficiency, respectively.

Table 3. Precision of the MPPT techniques.

P&O	*IC*	*PSO*	*FLC*	*KF*
98.2%	99.3%	99.0%	98.6%	99.4%

5.3 Ability to deal with shadow

From the analysis of Fig. 12(a) to 12(e), it is clear that only the PSO algorithm is able to reach the global MPP in partial shadow situation, since it is based on the exploratin and exploitation of the research space (starting from 40 V). Following the same protocol, the other MPPT algorithms end operating around a local MPP. Table 4 summarizes these results.

Table 4. Ability to deal with partial shadow.

P&O	*IC*	*PSO*	*FLC*	*KF*
No	No	Yes	No	No

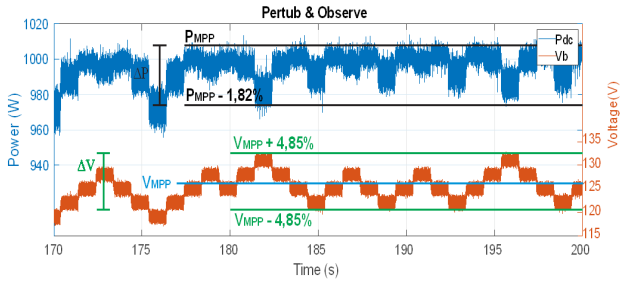

(a) Using P&O

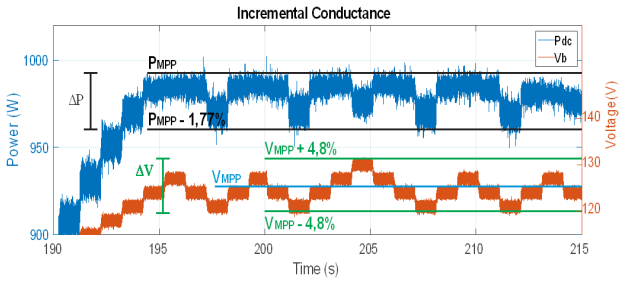

(b) Using IC

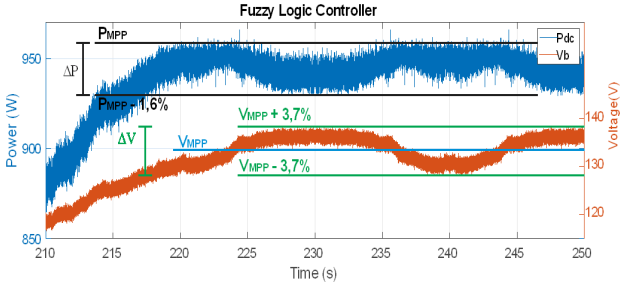

(c) Using FLC

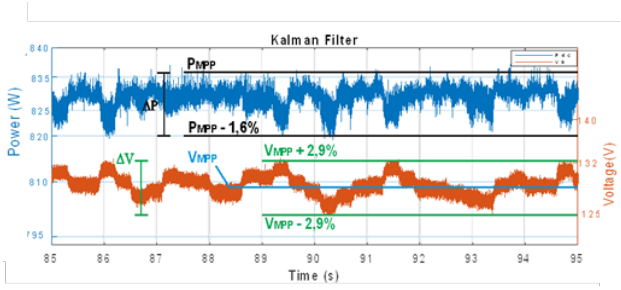

(d) Using KF

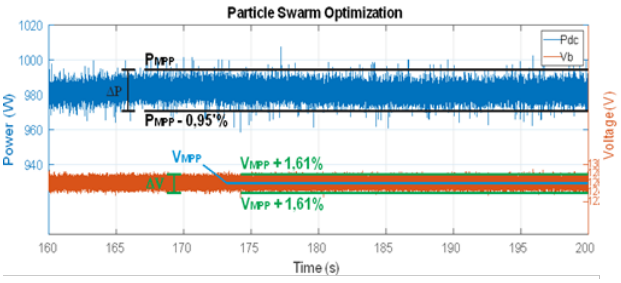

(e) Using PSO

Fig. 13. Oscillation of the MPPT algorithms at the MPP.

6. Conclusion

This work presented an experimental evaluation of five MPPT algorithms: P&O, IC, PSO, FLC and KF. This comparative study evaluated the performance of the algorithms in relation to 3 parameters: the accuracy of the MPP found in relation to the previously known value; the maximum oscillation of the power extracted from the PV string; and the ability to find the global MPP under the shadow effect. The experimental results show that the KF and IC algorithms operate closer to the MPP than the others. In this case, their efficiency is 99.4% and 99.3%, respectively. However, the PSO algorithm has less oscillation (0.95%) around the MPP compared to the others.

Despite using different methods of different complexity to find the MPP, the difference in efficiency obtained with the techniques was less than 2% under normal operating conditions. However, under partial shadow situations, the efficiency may increase with the PSO since it was the only one that demonstrated to be able to find the global maximum.

References

[1]. P. S. Pai, and S. Beevi, "Dual maximization of solar power for medium power application", 2013 International Conference on Renewable Energy Research and Applications (ICRERA). IEEE, 2013.

[2]. D. Yousri, T. S. Babu, D. Allam, V. K. Ramachandaramurthy and M. B. Etiba, "A novel chaotic flower pollination algorithm for global maximum power point tracking for photovoltaic system under partial shading conditions", IEEE Access 7 (2019). 121432-121445.

[3]. S. Wall, H. Xiao-Cong, L. Sha, and J. Xie, "High-efficiency PV inverter with SiC technology", 5th IET

Renewable Power Generation Conference, vol. 12, pp. 149-156, 2017.

[4]. N. Eswar, "Performance Study of Incremental Conductance and Modified Incremental Conductance MPPT Algorithms for Photovoltaic Applications", International Journal of Science- Engineering and Technology Research (IJSETR), Vol. 5, March 2016.

[5]. D. Yousri, T. S. Babu, D. Allam, V. K. Ramachandaramurthy, E. Beshr, and M. B. Eteiba. "Fractional chaos maps with flower pollination algorithm for partial shading mitigation of photovoltaic systems", Energies 12.18 (2019): 3548.

[6]. M. Abdulkadir, A. L. Bukar and B. Modu, "Mppt-based control algorithm for PV system using iteration-PSO under irregular shadow conditions", Arid Zone Journal of Engineering- Technology and Environment, Vol. 13, February 2017.

[7]. V. K. Viswambaran, A. Ghani, and E. Zhou, "Modelling and Simulation of Maximum Power point Tracking Algorithms & Review of MPPT Techniques for PV Applications", 5th International Conference on Electronic Devices, Systems and Applications (ICEDSA), pp. 1-4, 6-8 Dec 2016.

[8]. T. Esram, and P. L. Chapman, "Comparison of Photovoltaic Array Maximum Power Point Tracking Techniques", IEEE transactions on energy conversion, vol. 22, June 2007.

[9]. H. J. El-Khozondar, and R. J. El-Khozondar, "A review study of photovoltaic array maximum power tracking algorithms", Renewables: Wind. Water. and Solar, vol. 3, pp. 1-8, 18 February 2016.

[10]. A. K. Podder, "MPPT methods for solar PV systems: a critical review based on tracking nature", IET Renewable Power Generation, vol. 13, pp. 1615-1632, April 2019.

[11]. N. Eswar, "Performance Study of Incremental Conductance and Modified Incremental Conductance MPPT Algorithms for Photovoltaic Applications", International Journal of Science- Engineering and Technology Research (IJSETR), Vol. 5, March 2016.

[12]. A. Belkaid, I. Colak, and K. Korhan. "Implementation of a modified P&O-MPPT algorithm adapted for varying solar radiation conditions", Electrical Engineering, 99(3), 2017, 839-846.

[13]. A. I. Nusaif, and A. L. Mahmood, "MPPT Algorithms (PSO, FA, and MFA) for PV System Under Partial Shading Condition, Case Study: BTS in Algazalia, Baghdad", International Journal of Smart Grid-ijSmartGrid, 4(3), 2020, 100-110.

[14]. J. Cubas, and S. Pindado, "Accurate Simulation of MPPT Methods Performance When Applied to Commercial Photovoltaic Panels", The Scientific World Journal, June 2015.

[15]. S. Motahhir, A. Aoune, A. E. Ghzizal, S. Sebti, and A. Derouich, "Comparison between Kalman filter and incremental conductance algorithm for optimizing photovoltaic energy", Renewables: Wind. Water. and Solar, pp, 1-10, vol. 4, 2017.

[16]. B. O. Kang, "Kalman Filter MPPT Method for a Solar Inverter", IEEE Power and Energy Conference. Illinois, pp. 1-5, 2011.

[17]. O. B. Belghith, L. Sbita, and F. Bettaber, "Maximum Power Point Tracking by the technique of the extended Kalman filter", International Conference on Green Energy Conversion Systems (GECS), pp. 1-5, 2017.

[18]. T. F. Guimarães and V. Leite, "Analyses of MPPT Algorithms in Real Test Conditions", 9th International Conference on Renewable Energy Research and Application (ICRERA). Glasgow, pp. 164-169, September 2020.

[19]. P. Bhatnagar, and R. K. Nema, "Maximum power point tracking control techniques: State-of-the-art in photovoltaic applications", Renewable and Sustainable Energy Reviews 23, pp. 224-241, July 2013.

[20]. A. K. Gupta and R. Saxena, "Review on widely-used MPPT techniques for PV applications", 2016 International Conference on Innovation and Challenges in Cyber Security (ICICCS-INBUSH). Noida, pp. 270-273, 2016.

[21]. A. Belkaid, U. Colak, and K. Kayisli. "A comprehensive study of different photovoltaic peak power tracking methods", 2017 IEEE 6th International Conference on Renewable Energy Research and Applications (ICRERA). IEEE, 2017.

[22]. M. A. Abdourraziq, M. Ouassaid, M. Maaroufi and S. Abdourraziq, "Modified P&O MPPT technique for photovoltaic systems", 2013 International Conference on Renewable Energy Research and Applications (ICRERA).

[23]. A. Farayola, Y. Sun, and A. Ali, "ANN-PSO Optimization of PV Systems Under Different Weather Conditions", 2018 7th International Conference on Renewable Energy Research and Applications (ICRERA).

[24]. K. Ishaque, Z. Salam, M. Amjad and S. Mekhilef, "An improved Particle Swarm Optimization (PSO)–Based MPPT for PV with reduced steady-state oscillation", IEEE Transactions on Power Electronics, vol. 27, pp. 3627-3638, August 2012.

[25]. C. K. Chui, and G. Chen, "Kalman Filtering with Real-Time Applications", Springer International Publishing. Berlin. Germany, 2017.

[26]. B. Bendib, F. Krim, H. Belmili, M. F. Almi and S. Bolouma, "An intelligent MPPT approach based on neural-network voltage estimator and fuzzy controller, applied to a stand-alone PV system", IEEE 23rd International Symposium on Industrial Electronics (ISIE). Istanbul, 2014, pp. 404-409, 2014.

[27]. D. Haji and N. Genc, "Fuzzy and P&O Based MPPT Controllers under Different Conditions", 7th International Conference on Renewable Energy Research and Applications (ICRERA). Paris, pp. 649-655, 2018.

[28]. V. Leite, Â. Ferreira and J. Batista, "Bidirectional vehicle-to-grid interface under a microgrid project", IEEE 15th Workshop on Control and Modeling for Power Electronics (COMPEL). Santander, pp. 1-7, 2014.

[29]. M. Breve, and V. Leite, "Control of a Bidirectional Single-Phase Grid Interface for Electric Vehicles", Ibero-American Congress of Smart Cities. Springer, Cham, 2019.